LUND UNIVERSITY
Faculty of Science

The effects of salt addition on the thermo-optical properties of soot

Amanda Kaarna

Thesis submitted for the degree of Master of Science
Project duration: 5 months

Supervised by Thi Kim Cuong Le and Saga Bergqvist

Department of Physics
Division of Combustion Physics
May 2024

Abstract

Soot is a known contributor to climate change due to its strong light absorption possibility. It has been shown that adding alkali salts during the soot formation reduces its soot absorption ability, and thus reduces its impacts, but the exact mechanics are not fully understood. This thesis aims to get a better understanding of the effects that salts have on soot. The salts used were sodium chloride and potassium chloride. Raman spectroscopy and thermo-optical analysis were used to gather data on soot samples. The resulting data from thermo-optical analysis was used to calculate the ratio of organic carbon and elemental carbon (OC/EC) ratio and mass absorption cross-section (MAC) of the samples. For the Raman spectroscopy measurements, the resulting spectra was deconvoluted into peaks and a fluorescence background. After the fluorescence background was subtracted from the data, the ratios of the various peaks were calculated to obtain knowledge of the graphitic structure. A comparison was made between the soot samples with salt from a Perkin-Elmer burner and soot samples with varying heights above a McKenna burner, as the height above the burner (HAB) has known effects on the soot sample's peak ratios. The differences between the soot samples are presented by plotting their Raman peak ratios I_{D_1}/I_G, I_{D_3}/I_G and $\ln(m/I_G)$ obtained from the Raman spectroscopy experiment, in which D_1, D_3 and G are Raman peaks of soot and m is the slope of the fluorescence background. The soot samples with salt addition had overall smaller I_{D_1}/I_G, $\ln(m/I_G)$ and MAC, and had larger I_{D_3}/I_G and OC/EC compared to the regular soot sample. All of these results, except the lower $\ln(m/I_G)$, implies that the samples with salt addition are less light absorbing than the reference soot. Using the results from both burners, the connection between the OC/EC and MAC, I_{D_1}/I_G, I_{D_3}/I_G, and $\ln(m/I_G)$ are presented. OC/EC has a positive correlation with I_{D_1}/I_G and $\ln(m/I_G)$ (McKenna samples) and a negative relation with MAC and $\ln(m/I_G)$ (Perkin-Elmer samples). The connection for OC/EC and I_{D_3}/I_G was more uncertain, though the results seem to hint at a negative correlation. The results obtained are discussed further in the thesis.

Populärvetenskaplig sammanfattning

Sot är en produkt som kommer ifrån ofullständig förbränning av olika bränslen, som fossila bränslen och biogaser. Sot produceras därför, bland annat, i många av våra fordon, så sot släpps ut i stora mängder. Sot har en negativ påverkan på miljö och mänsklig hälsa. Det finns olika typer av sot. De som absorberar ljus bättre och har större klimatpåverkan kallas moget sot, medan sot med sämre ljusabsorptionsförmåga kallas omoget sot. Mogenheten på sotet beror på hur länge den varit i förbränningen, och mogenheten påverkar sotets olika egenskaper.

Sotets mogenhet brukar kategoriseras genom att titta på dess egenskaper. Ett exempel på en sådan egenskap är sotets komposition av kol. Kol i sot brukar uppdelas i två delar, det organiska kolet, som är kol blandat med andra organiska ämnen, och det elementära kolet, som kan anses vara rent kol. Mognare sot har mera elementärt kol. Ett annat sätt att kategorisera sotets mogenhet är att titta på dess nanostruktur, eftersom mognare sot har mer struktur.

I denna rapport studerades hur nanostrukturen och kompositionen av sot påverkas när salter tilläggs under sotets formation. Salterna som undersökts i den här studien är natriumklorid och kaliumklorid. Tidigare studier har konstaterat att additionen av dessa salter ger sämre absorptionsförmåga på sotet, men detta är ett relativt nytt forskningsområde, så flera studier behöver utföras.

Två olika tekniker används för att studera salternas påverkan på sotet. För att få information om nanostrukturen användes Ramanspektroskopi, som producerar ett spektrum från ljusets växelverkan med vibrationer eller rotationer i molekylernas bindningar. Detta spektrum är ett Ramanspektrum, och vad några av de olika topparna i Ramanspektrumet säger om nanostrukturen är känt. För att kompositionen ska kunna studeras användes termo-optisk analys, där sotet förångas i olika omgivningar för att separera kolet som sotet består av i organiskt och elementärt kol. Organiskt kol kan omvandlas under förångningen till pyrolytiskt kol, som anses ha liknande egenskaper som elementärt kol. Förångningen korrigeras med hjälp av transmission av lasrar igenom filtret som sotet är på. Detta är för att pyrolytiskt kol förbättrar sotets absorptionsförmåga, så transmissionen försvagas. Det inspekteras också hur förångningen påverkar sotets nanostruktur. Absorptionsförmågan för sotet kan räknas ut med parametrar ifrån den termo-optiska analysen.

Resultaten från Ramanspektroskopi experimentet indikerar att sot med salt i dess formering är mindre strukturerat, har mera amorft kol och har mindre bundet väte. Strukturen för de olika sot exemplaren utvecklades ungefär likadant under uppvärmningen. OC/EC ration av dessa exemplar var högre för soten med salt addition, och absorptionsförmågan var sämre för sot med salt tillagd i dess formering. Mindre bundet väte innebär bättre ljus absorptionsförmåga, men resten av resultaten indikerar sämre ljus absorptionsförmåga. Kaliumklorid verkade ha större påverkan på OC/EC, vätebindningen och MAC än natriumklorid. Sammanfattningsvis gör salt additionen att sot får en sämre absorptionsförmåga. Detta kan vara viktigt då salter används för att skapa biomassa, så det kan tyda på att mera salt ska läggas till för att reducera biomassans effekt.

Contents

List of acronyms

ATN, Attenuation
BC, Black Carbon
BrC, Brown Carbon
BWF, Breit-Wigner-Fano
CCD, Charge Couple Device
EC, Elemental Carbon
FID, Flame Ionization Detector
FWHM, Full Width at Half Maximum
HAB, Height Above Burner
LAC, Light Absorbing Compound
MAC, Mass Absorption Cross-section
OC, Organic Carbon
PAH, Polycyclic Aromatic Hydrocarbon
PC, Pyrolytic Carbon
TC, Total Carbon
TOA, Thermo-Optical Analysis

1 Introduction

How to reduce the impact on the environment from various sources, such as vehicles and energy, is currently a big topic. One big question is to reduce the use of limited resources and replace them with renewable materials instead. This is the main discussion for replacing fossil fuels. Not only do fossil fuels produce harmful byproducts into the atmosphere, they are also a limited resource which takes millions of years to produce. One renewable fuel which is a candidate for replacing fossil fuels is biomass. While biomass have benefits compared to fossil fuels, they still produce some of the same harmful byproducts, most notably soot.

Soot, which is sometimes called black carbon (BC) [1], is a carbonaceous substance emitted from the incomplete combustion of organic materials [2], which can be generated when various fuels, such as fossil fuels and biomass, are burned [3]. The process in which soot is formed can be described in stages, although these stages do not have a clear distinction [4]. The soot formation is shown in Figure 1. Firstly, throughout the soot formation, OH, O, H, CH and CH_2

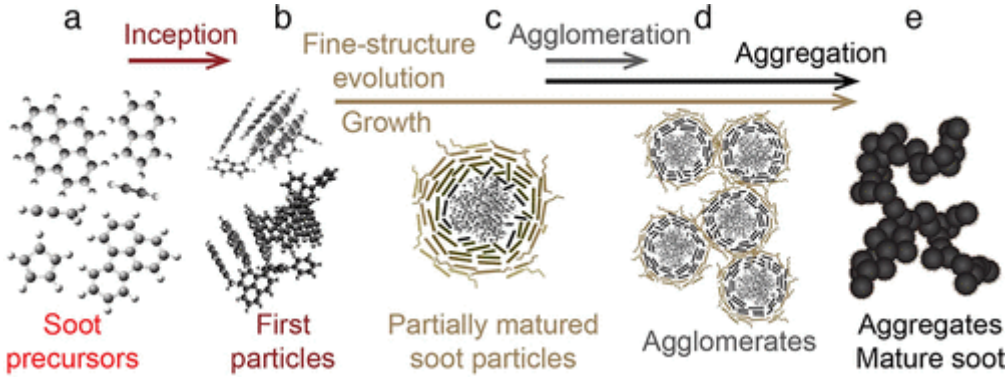

Figure 1: Image of the major steps in soot formation, with the scale of the images becoming larger for later steps. Image taken from Figure 1 in [4]

are important as they react to create soot precursors [5]. One such precursor to soot is Polycyclic aromatic hydrocarbon (PAH) molecules [3]. These molecules transition into condensed-phase particles (i.e, liquids and solids), which are incipient soot particles [4]. Due to high temperature, these particles evolve further as the hydrocarbons get converted into and replaced by pure carbon, improving the absorption so they can absorb visible and infrared wavelengths [4]. As they evolve, the particles collide with each other, forming agglomerates, which eventually get stronger bounds, forming aggregates [4]. These aggregates are known as mature soot and absorb light better than the incipient soot particles. Mature soot particles are usually around 10-50 nm and incipient particles are 1-3 nm [6]. Also, the more mature soot becomes, the more graphitized and ordered it will become [2].

Soot is a health hazard, as research has shown that soot particles that are coarse, fine and ultra-fine all can have adverse health effects, though for different reasons [7]. Not only that, but ultra-fine fractions can penetrate the lung lining and get inside the blood, where they can move to other organs and cause cardiovascular diseases [7]. From these health effects, it is clear that soot can increase the mortality rate [2, 7]. Soot is a known air pollutant, which is another reason why it causes health problems in the human population. Soot can also give air pollution by reacting to the O_3, NO_2 and SO_2 in the air, which can cause respiratory problems and other health issues [5].

Soot also contributes to the global warming of Earth's atmosphere and on its surface, as soot is a light absorbing compound (LAC) [2] that absorbs light and converts it into heat [8]. The effects of soot are divided into four categories, the direct effect, as just described, the indirect effect, the semi-direct effect and the indirect surface albedo effect [7]. In general, the direct effects are more important compared to the other effects because they contribute a positive radiative

forcing. A positive radiative forcing usually means an increase in temperature for the climate, whereas indirect effects can give a negative radiative forcing [1, 7]. An example of an indirect effect is soot influencing cloud processes [7, 5]. The cloud process is disturbed because the soot particles can act as ice nucleating particles, which are important during cirrus cloud formation [9]. The semi-direct effect is due to soot affecting the heating rate over a certain region, changing that region's humidity which in turn affects if clouds can be formed or sustained there [7]. The indirect surface albedo effect occurs because the surface albedo of snow and ice get affected when soot settles on those surfaces [5]. Not only does BC affect the surface albedo, but so does absorbing organic carbon [10], so even less mature soot can have a significant effect. Soot is in fact twice as effective as carbon dioxide at altering the surface air temperature through this process [11].

The total radiative forcing from these effects is estimated to be +0.11 W m^{-2}, or between -0.2 to +0.42 W m^{-2} due to uncertainty [1], and it is possible that the radiative forcing is higher at specific locations [7]. Another concern is that soot gathers in the atmosphere over areas, such as oceans and the Arctic, which are far away from most of the known sources of soot [7]. Because of these environmental factors, soot is considered a main contributor to global warming alongside carbon dioxide and methane [12].

Because of soot's effects and the fact that it is found in abundance when combusting fuel, researchers have an interest in studying soot and its properties. While a lot of progresses have been made, there are still many questions about soot that are unanswered [13]. To study soot, various techniques can be employed. One such technique is Raman spectroscopy. This method can be used to gather information of the nanostructure of carbonaceous materials [13]. In particular, due to Raman spectroscopy being sensitive to the molecular and crystal structure of the material, it is very useful for studying disordered carbon materials, such as soot [2, 14]. The results from a given Raman measurement can provide structural information of the soot sample, such as its graphite and amorphous structure, based on the peak positions, peak widths and peak intensity ratios [6, 14]. These results also suggest the maturity of the soot, as mature soot is more ordered.

Raman spectroscopy is a common method for studying carbonaceous materials, as it can be used to study the structure and chemistry of the materials in a wide variety of environments and conditions [15]. Raman spectroscopy is also nondestructive [2], and can be performed on carbon samples either in the aerosol phase (online) or on substrates (ex situ), giving this technique more versatility and many applications. For instance, it can be used to see how carbon black, an industrial carbon material used for many applications, such as reinforcing rubber or as a pigment, changes during a heat treatment [16], or to map graphenes membranes [17].

Another method for characterising soot properties is to use thermo-optical analysis (TOA), from which the OC/EC ratio can be obtained. This is the ratio between organic carbon (OC) and elemental carbon (EC) [18]. The total carbon (TC) of soot is split into these two different components, which describe the amount of EC and OC in the material. EC is carbon mixed with other materials that make up a significantly smaller part of the material compared to the carbon, so EC can be considered to be just carbon [4]. In OC, the non-carbon materials are more noticeable. OC is therefore considered as carbon mixed with other materials. The other elements can be, for instance, hydrogen, oxygen and nitrogen [4]. Both types of carbon absorb light, but EC absorbs a broad range of light (300-1000 nm [20]) and OC usually absorbs in the ultraviolet and infrared regions [4]. However, some OC absorb shorter wavelengths better than EC, which are known as brown carbon (BrC), which absorbs strongly within the wavelength 400 to 700 nm [21]. Because EC generally means better absorption, the OC/EC ratio not only gives some clues about the composition of the soot, but also its maturity. A higher OC/EC ratio could also suggest a lower impact on global warming, as OC generally gives a negative radiative forcing, estimated to be –0.21, or in the range –0.44 to +0.02 due to uncertainty [1].

It has been suggested that reducing the contribution of BC could help to keep the global

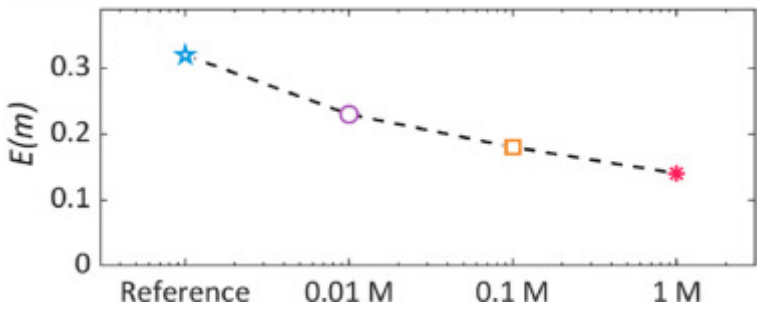

Figure 2: Graph showing how the light absorption function $E(m)$ is affected by the addition of potassium chloride. Graph is Figure 2 (b) from [13]

warming at 1.5°C in the short-term [1]. It has also been shown that the addition of potassium chloride during soot formation significantly reduces the light absorption efficiency of soot [3, 12, 13]. This is also seen in Figure 2, where more salt is also shown to reduce the light absorption of the soot sample. The exact mechanics for this reduction is still not fully understood, and more research needs to be done. Therefore, in this paper, how the nanostructure and composition in soot changes with potassium - or sodium chloride added during the soot formation is studied. The structure is studied by using ex situ Raman spectroscopy and the composition can be studied by using the OC/EC ratio. It is also of interest to see how heating the samples changes the structure of them, as the addition of salt could change how the parameters evolve during heating.

2 Method and Experiment

2.1 Sample preparation

All of the soot samples used in this study were collected on quartz filters. These samples were prepared by adding sodium chloride or potassium chloride into the flame of a Perkin-Elmer burner at a height of 14 mm above the burner. The samples were created by letting soot gather on the quartz filters for 20-30 minutes. The flames were premixed, meaning they consist of a mixture of air and a fuel, with ethylene (C_2H_4). The mixture was made up of C_2H_4 and air, with equivalence ratio $\Phi = 2.6$. There was also a co-flow air. The Perkin-Elmer burner (Figure 3) has a spray chamber that has three connections, which are for fuel, auxiliary air and nebulizer air, with the nebulizer connection used for implementing the salt solutions into the flames [24]. The nebulizer was connected to deionized water in which various salts can be dissolved. Three soot samples were generated with the Perkin-Elmer burner; one where just the regular flame, where regular deionized water was connected to the nebulizer, was used and the rest of the samples had salt solutions connected to the nebulizer. The other two samples had 1 Molar of salt added to the water, one sample having NaCl and and the other having KCl. The setup for the Perkin-Elmer burner was similar to the McKenna burner, which is described below.

Before using these samples, soot samples prepared with a McKenna burner (Figure 3) were used for testing the experimental setup and to test the data analysis. The flames were premixed and C_2H_4 was used as fuel. The premix has an equivalence ratio of $\Phi = 2.1$ and the same coflow was used as the one in the Perkin-Elmer burner. The setup of a McKenna burner, and also the Perkin-Elmer burner, is described in [18], where there was a probe at a specific height above the burner (HAB) with an orifice where the generated soot could enter the probe. There was also a stabiliser plate above the probe to stabalize the flames. The soot was transported through the tube by N_2 and collided and gathered on a filter placed in a filter holder further away. The studied HAB's used were 9 mm, 12 mm and 15 mm. The maturity of the soot sample increases with increasing HAB [5]. No other parameter was changed, so there is only one dimension of

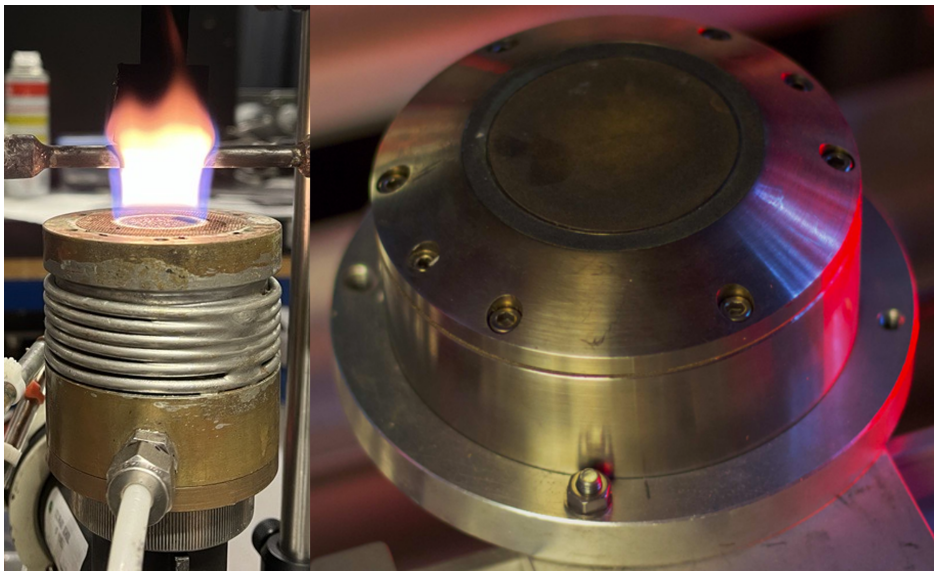

Figure 3: (left) A Perkin-Elmer burner. Picture courtesy of Saga Bergqvist. (right) A McKenna burner. Picture courtesy of [25].

concern that differs between the samples. The samples used in this study are shown in Figure 4.

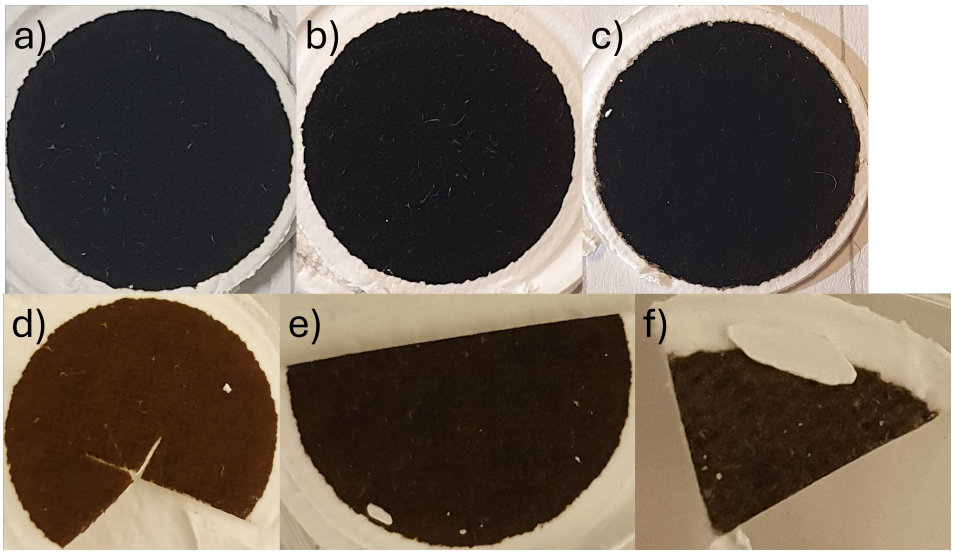

Figure 4: (top) Samples from the Perkin-Elmer burner. (a) Reference sample. (b) NaCl sample. (c) KCl sample. (bottom) Samples generated with the McKenna burner. (d) 9 mm HAB. (e) 12 mm HAB. (f) 15 mm HAB.

2.2 Raman spectroscopy

Raman spectroscopy works by observing the Raman scattering of light from a sample. The Raman scattering occurs when a sample is excited into a virtual state and becomes de-excited to a different energy level than the one it was excited from [19]. The scattering can be categorised into two different parts, anti-Stokes and Stokes scattering. The Stokes Raman scattering is when the photon emitted from the de-excitation is redshifted (meaning the molecule de-excites into a higher state than before it was excited), and in anti-Stokes Raman scattering, it goes to a lower

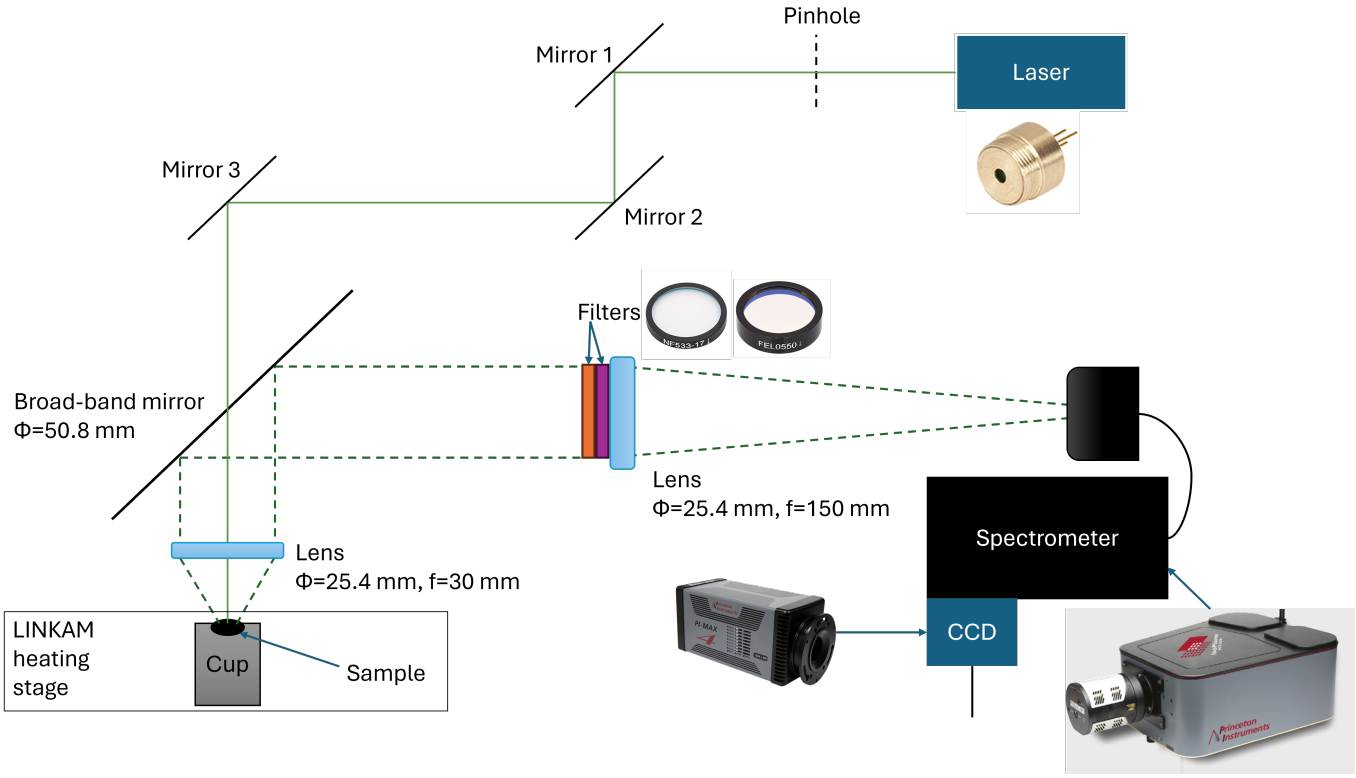

Figure 5: The setup of the experiment and pictures of the components used. The marked cup is a ceramic cup, f is the focal length and Φ is the diameter of the optical component. Image is inspired by Figure 1 from [6]. The pictures of the filters and laser diode are courtesy of ThorLabs and the pictures of the CCD camera and spectrograph are courtesy of Teledyne Princeton Instruments.

energy level and the photon is therefore blueshifted [19].

Ex situ Raman spectroscopy was used. The excitation wavelength used for the laser was 532 nm, one of the most common lasers for Raman spectroscopy of soot. The soot sample was put into a LINKAM heating stage, which can be filled with gases and heat whatever is inside it. The setup in the LINKAM heating stage for Raman spectrometry was similar to that found in [6]. A schematic of the setup is shown in Figure 5, and the actual setup is shown in Figure 6. First, a pinhole was used to reduce the scattering of the laser before it came onto a set of mirrors. This set of mirrors was implemented for steering the laser into the heating stage where the samples were placed. A broadband mirror, with a diameter (d) of 50.8 mm, was placed in front of the heating stage and had a hole in it so that the incoming light could pass through it. The laser beam passed this mirror and was focused onto the sample by a lens, with a focal length (f) of 30 mm, and d=25.4 mm. Before any measurements were done, the lens was set so that the best focus was achieved, which was done by looking at different positions of the lens and fastening it at the position which seemed to give the best focus. Afterwards, the sample itself was moved around so that the laser was aimed as close to the middle of the sample as possible. The scattered light in the stage went out and was collimated by the same lens onto the broadband mirror. The laser then went through another lens (f=150 mm, d=25.4 mm) to focus it on the detection device.

However, not all of the scattering that was emitted from the sample is of interest for this experiment, so two filters were implemented to remove those wavelengths. One filter used was a notch filter, ThorLabs NF533-17. The filter removes the Rayleigh scattering, the scattering where the excited soot returns to its original state. This scattering is uninteresting for the purposes of this study, and the Rayleigh scattering's high intensity compared to Raman scattering

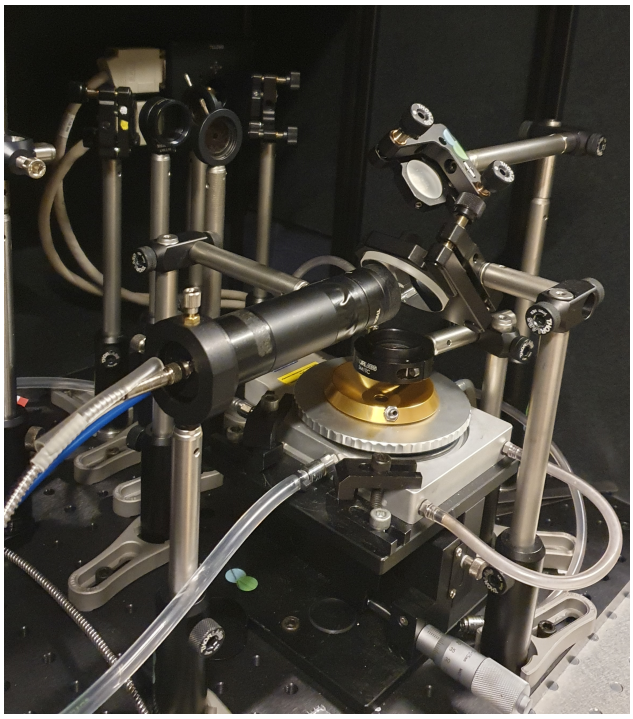

Figure 6: The setup used for performing Raman spectroscopy.

could damage the light-sensitive equipment. A long wave pass edge filter, ThorLabs FEL0550, was also put into the setup. This was to remove anti-Stokes Raman scattering, as that region is not interesting for the purposes of this paper. Interesting regions where the characteristic peaks of soot in the Raman spectrum are found at Raman shifts above 800 cm^{-1} [6, 14]. How much light these filters transmit at different wavelengths is shown in Figure 7.

To record the data, a charge coupled device (CCD) camera was used. The intensity from Raman scattering was weak compared to the light from the environment, so the setup needed to be covered up to minimize the light that entered into the camera to reduce any outside noise. Each Raman measurement was made with 20 acquisitions, each taking 25 seconds.

Table 1: Some of the first order peaks observed in the Raman spectrum of soot, their position in the spectrum and what vibrational mode they correspond to.

Peak	Approximate Raman shift (cm^{-1})	Vibrational mode
G	1590-1620 [6]	Stretching of pairs of sp^2 carbon atoms [22]
D_1	1350 [6, 14, 22]	Comes from defects, and starts the breathing modes of the sp^2 carbon in aromatic rings [22]
D_2	1620 [14]	Lattice vibration of the graphene layers on the surface of a graphitic crystals [14]
D_3	1500 [6, 14, 22]	Amorphous sp^2 phase [22]
D_4	1170 [22]	Trans-polyacetylene section in grain boundaries [22]
D'_1	1270 [6]	Not known, but it is suggested that it could come from a merging polyaromatic subunits from organic compounds [6]
C_1	1800-2000 [6]	Polycumulene, an sp hybridization state [6]

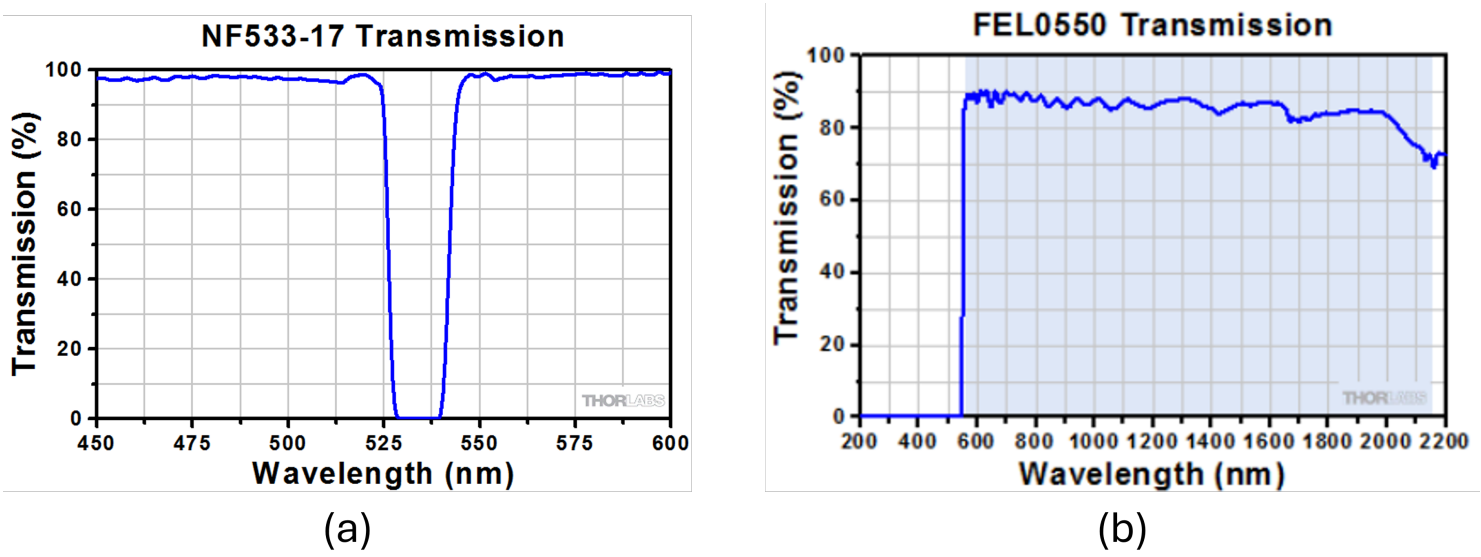

Figure 7: (a) The transmission graph for the notch filter. (b) The transmission graph for the long wave pass edge filter. Graphs courtesy of ThorLabs.

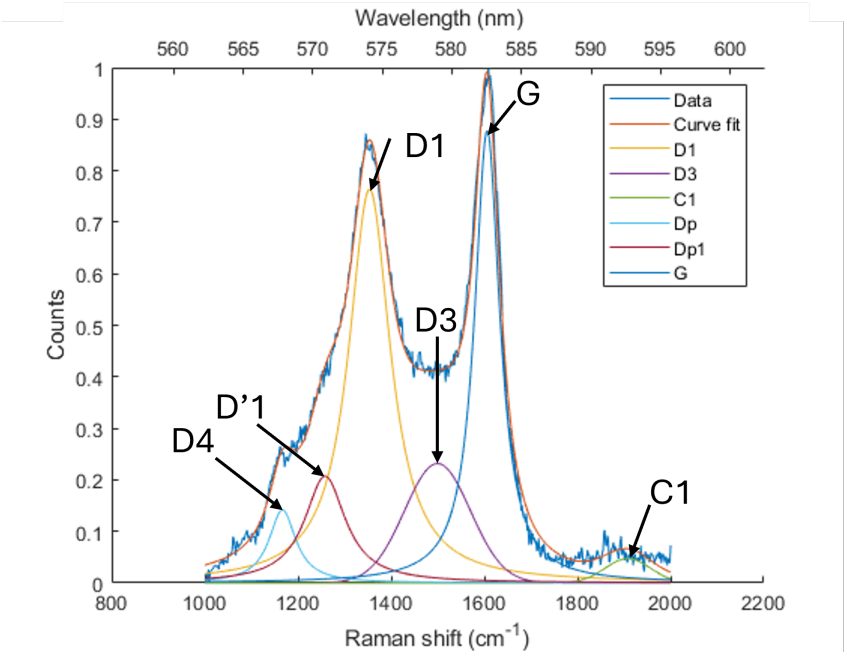

Figure 8: The deconvoluted Raman spectrum of an untreated KCl soot sample with the characteristic peaks marked.

Using Raman spectroscopy, the measurement yields a spectrum. This spectrum for a soot sample has a characteristic appearance, with some characteristic peaks at specific Raman shifts in the spectrum, as shown in Figure 8. The Raman shift is defined as

$$\Delta\nu = (\frac{1}{\lambda_0} - \frac{1}{\lambda}) \cdot 10^7, \tag{1}$$

where $\Delta\nu$ is the Raman shift, λ_0 is the excitation wavelength of the laser and λ is the wavelength emitted when the sample is de-excited. The multiplication with 10^7 is to express the Raman shift in cm^{-1} when the wavelengths have the unit nm. This formula can be used to convert the

Raman shift into wavelength, as done in Figure 8.

The peaks in the spectrum can be deconvoluted from the data and have specific labels and indicates properties that the soot has. The peaks that are relevant for this study and what they suggest about the samples are given in Table 1.

Table 2: The heating steps of EUSAAR_2. The modified time is the time that the temperature was held constant when the heating scheme was used in the LINKAM heating stage.

Step	Temperature (°C)	Time (s)	Modified time (s)
OC1	200	120	60
OC2	300	150	120
OC3	450	180	135
OC4	650	180	120
EC1	500	120	120
EC2	550	120	105
EC3	700	70	25
EC4	850	80	35

To get data of the structure of the soot sample, a measurement was performed in the LINKAM heating stage in an N_2 environment at an ambient temperature. There was an interest in knowing how heating influences the Perkin-Elmer samples, so the samples were heated. The laser was blocked during the heating process, as the laser could oxidize the sample when it was heated. The heating process used in the LINKAM heating stage was similar to EUSAAR_2 [26], although instead of He, N_2 was used, as it is a less expensive gas and it works as an inert environment for the purposes of this paper. The heating procedure in the DRI is the regular EUSAAR_2, and and the procedure's steps are shown in Figure 9. The heating scheme works by having the sample heated at different temperatures at various intervals in an inert environment and then in an inert atmosphere with O_2 making up 2% of the environment. Cavalli et al. [26] gives the time at which the temperature is increased to and held at a specific temperature. These different heating steps are presented in Table 2.

In the LINKAM heating stage, a temperature, increase rate and time that the set temperature is held at can be chosen. However, the time for each step in EUSAAR_2 includes the time it takes to heat up the sample to the constant temperature, with the exception of the EC1 step, as seen in Figure 9. The time used in the LINKAM heating stage therefore needed to be calculated. The increase rate for all the steps was 200°C/min, and using that and the times given in EUSAAR_2 scheme, the times for the constant temperature at each step were calculated. The first heating step, OC1, starts at an ambient temperature and goes to 200°C, so the temperature is kept constant for 60 s, if it is assumed that the temperature starts at 0°C rather than somewhere between 20-30°C. The rest are shown in Table 2. Between each heating step, the sample was left to cool down so a Raman measurement could be performed at room temperature. This is because the laser can oxidize the sample if it is too warm. The O_2 added during the heating was also removed during measurements so the environmental conditions for the measurements were the same and to make sure that the laser did not accidentally oxidize the soot sample. The measurements were done at room temperature, around 20-40°C.

To add O_2 into the system, normal air (as normal air is cheaper and in larger quantities than pure O_2) was used and it was taken into account that air consists of approximately 70% of N_2. Two mass flow controls were used to regulate the flow of the two gases into the heating stage. A valve was placed before the mass flow controller responsible for regulating the air, so it could easily be turned off during the Raman measurements. The valve was opened when the

heating starts for a heating step which requires O_2, and was closed when the heating step was completed.

For each heating step, some soot from the filter will be evaporated. This means that the background noise from the filter becomes stronger over time, which affects the resulting Raman spectrum. Because the filter is always present, it can give some background to the data even when the sample has not been heated beforehand. This can happen if the beam is focused on the filter rather than the thin layer of soot. To correct for the filter, an empty quartz filter went through the same heating procedure with breaks to perform Raman measurements. The reason the filter went through the same process as the samples is because the heating procedure could affect the filter too. The gathered data could then be used to remove the effects of the filter from the spectra.

For each sample, the experiment was done at two different parts of the sample. This was done because there could be local variations on one part of the filter. Taking more measurements could help to reduce and correct for these local variations. It also gives a more accurate Raman spectrum when the spectra are summed and averaged. The background was measured when the laser was turned off and was subtracted from all of the Raman spectra.

2.3 Thermo-optical analysis

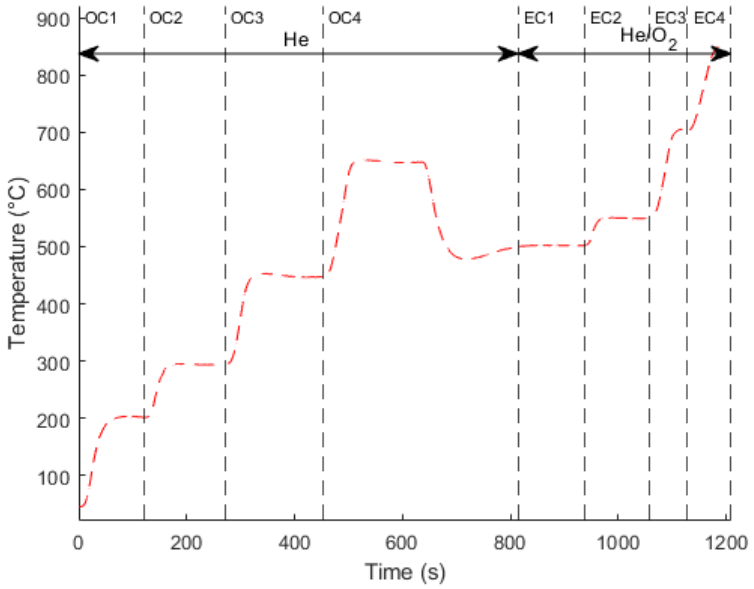

Figure 9: The EUSAAR_2 heating protocol in details. The steps taken are marked as well as the chemical composition of the environment in which the sample is heated

To analyze the composition of the soot, the OC/EC ratio was employed. The ratio implies the maturity of the soot, as mature soot has more EC and less OC. To determine OC and EC, a heating procedure was used on a soot sample collected onto a quartz filter. The details for these procedures differ, but they all follow the principle that there is first heating done in an inert atmosphere of He, and later heating in an inert environment mixed with some O_2. An example of such a procedure is shown in Figure 9. OC is defined as the carbon emitted in the inert environment and EC is defined as the emitted carbon in the environment with a small fraction of oxygen [18]. A separate team used an instrument known as DRI 2015, shown in Figure 10a, to collect the data used to calculate the OC/EC ratio. The method used by the team is described in [20], and the setup is shown in Figure 10b.

The principle of the method is to measure the reflectance and transmission of the lasers, as

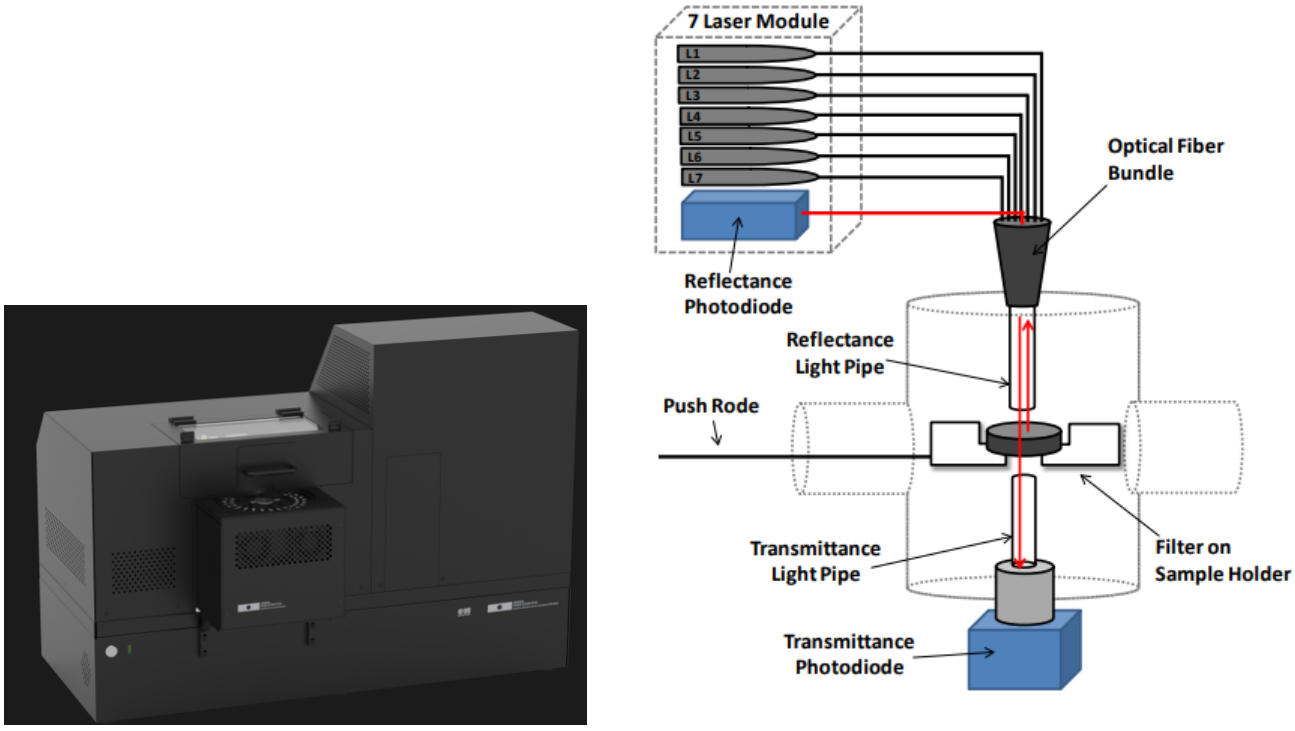

(a) (b)

Figure 10: (a) A DRI 2015. Picture created by Aerosol magee scientific. (b) A schematic of the DRI 2015. Image is Figure 1 from [20].

well as the carbon detected with a flame ionization detector (FID) from heating the sample. The temperatures during the heating are usually at a magnitude of 100°C, and oxygen is usually injected at the later temperatures to remove the EC from the sample. The sample was put in a holder and seven diode lasers of various wavelengths (405, 450, 532, 635, 780, 808, and 980 nm) were directed to the sample with a light pipe, a type of optical fiber. The choice of wavelengths of the lasers was because the light used should be for the visible light to near infrared, and the limit of what lasers are commercially available [20]. These lasers were pulsed so an individual laser gave two pulses before the next laser did the same. An eight-furcated optical fiber bundle was used to send the lasers into the light pipe, one for each laser and one for directing the reflected light from the filter towards a photo-diode. There was also a light pipe after the filter to direct the light onto another photo-diode to detect the transmitted light. To minimise the noise, the product between the detected and reference signal was integrated by an NI6216 data acquisition system. After the heating scheme was completed, a known amount of methane was injected into the analyzer to calibrate the FID signal [18]. Only the 635 nm laser is presented in this study, as the organic material absorbs light best at values below 700 nm, if it absorbs anything at the visible light at all. In either case, the pyrolysis of the OC changes the absorption significantly around 700 nm. Therefore the wavelength closest to 700 mm should be used.

The detection of the carbon by the FID is done by having the evaporated carbon become oxidized into CO_2 [23]. From here, the CO_2 can be reduced into CH_4 and get detected by the FID [23]. Due to this process, there is a delay between when the carbon is detected compared to its corresponding laser transmission. The delay time in the experiment is 20 seconds.

The heating scheme used for gathering OC and EC was the unmodified EUSSAR_2 protocol, to remove the OC and EC and see how the transmission of light changes. To analyse the resulting data, thermograms were made in which the data is plotted, an example is shown in Figure 11. These have the temperature, the normalised transmission and adjusted carbon plotted in the

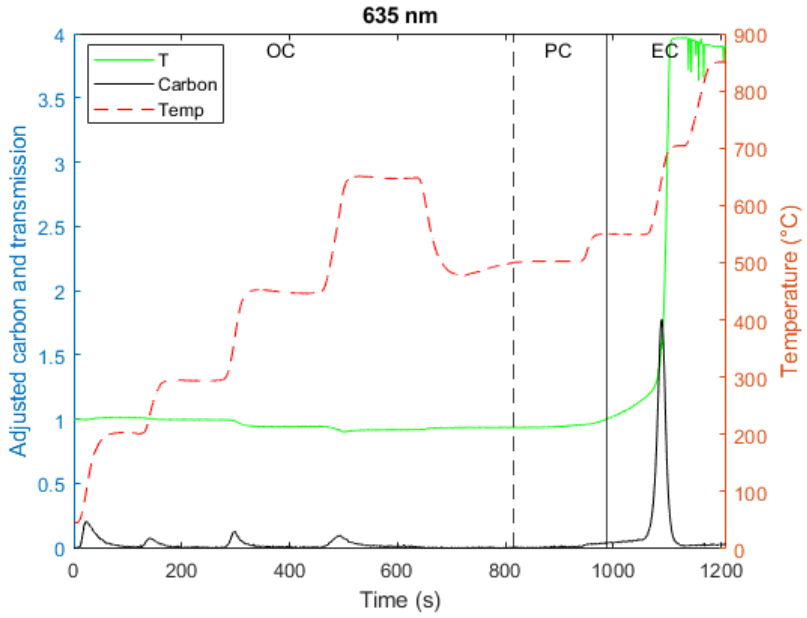

Figure 11: Thermogram for a the reference soot from the Perkin-Elmer burner. T stands for the transmission, Carbon for the FID signal of carbon and Temp stands for the tempreature. The dashed line shows where the EC steps begin and the regular black line shows where the PC is depleted. The FID signal is adjusted to make both the transmission and FID signal visible. The OC/EC ratio is unaffected by this adjustment.

same graph. The transmission coefficients were normalised with respect to its value at the start of the procedure. This was to correct for the OC converted into PC through pyrolysis during the heating. The correction works by assuming that PC have optical properties similar to EC and evolves at lower temperatures [18], and it therefore decreases the transmission of the laser. The carbon detected during the oxidized atmosphere (i.e., after the black vertical dashed line in Figure 11) will therefore be both converted OC and EC. To correct for this, and using that the PC is gathered on the filter, EC will not be counted until the transmission has the same value it has at the start of the measurement (i.e., after the vertical black line in Figure 11), when it is clean from PC.

2.4 Data analysis

2.4.1 Data treatment of Raman spectra

When measuring the Perkin-Elmer samples, it was observed that there was a difference between the samples when the glass lid of the heating stage was on or removed, as seen in Figure 12a. To take this difference into account, two measurements were made in an air environment, no oxidation occurs here for the samples used, first without a lid and then with a lid. The ratio between these measurements (lid removed / lid on), shown in Figure 12b, was multiplied with the different steps of the data.

For the Raman data, it was sometimes noticed that very large and thin peaks were randomly scattered in the Raman spectrum, as shown in Figure 13a. This is because Raman spectroscopy is sensitive, and that includes a sensitivity to cosmic rays that can randomly get detected by the CCD camera. To solve these disturbances in the data, a despiking algorithm is used to remove these data points. Not all of the cosmic rays are removed by this algorithm, however, as can be seen in Figure 13b. This is usually not a problem, as the cosmic ray is in a region that is not interesting for the deconvolution of the spectrum. There are some exceptions, though, but these do not affect the parameters obtained from the deconvolution significantly, aside from the

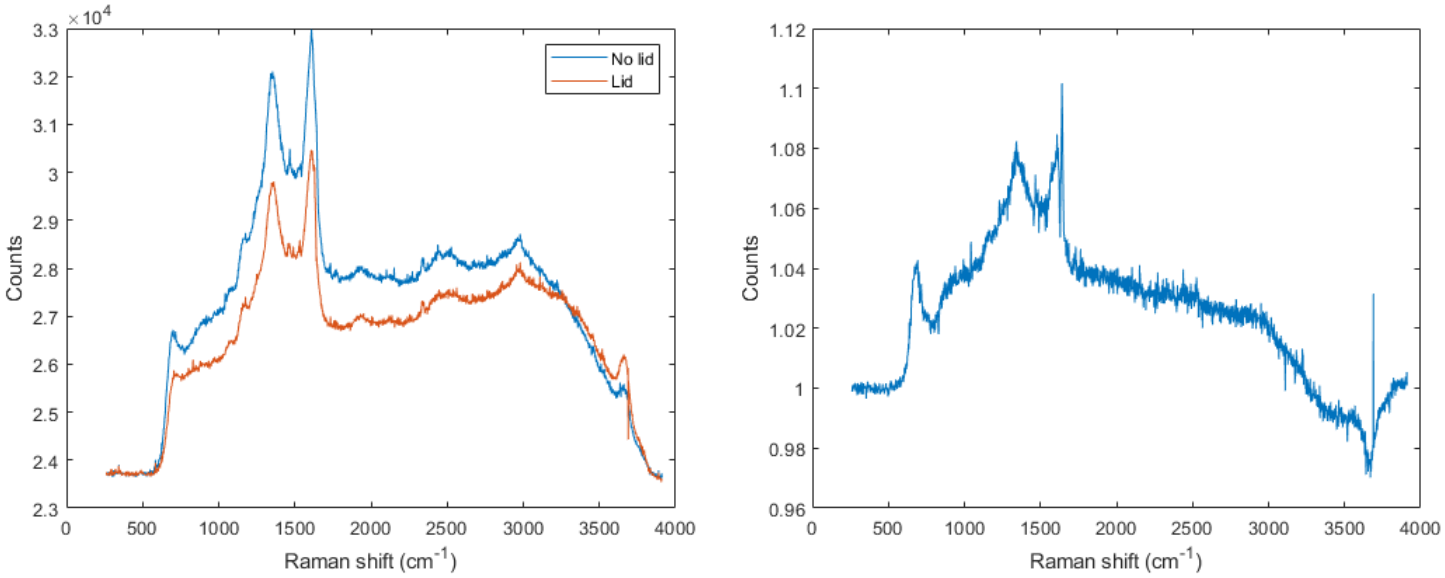

(a) (b)

Figure 12: (a) The despiked Raman spectra, either with or without the lid. (b) The ratio between the Raman spectra of when the lid is on the stage or removed from the stage.

parameter that shows how accurately the data fitting describes the data, but that is not too relevant for the data analysis, so no further correction is done.

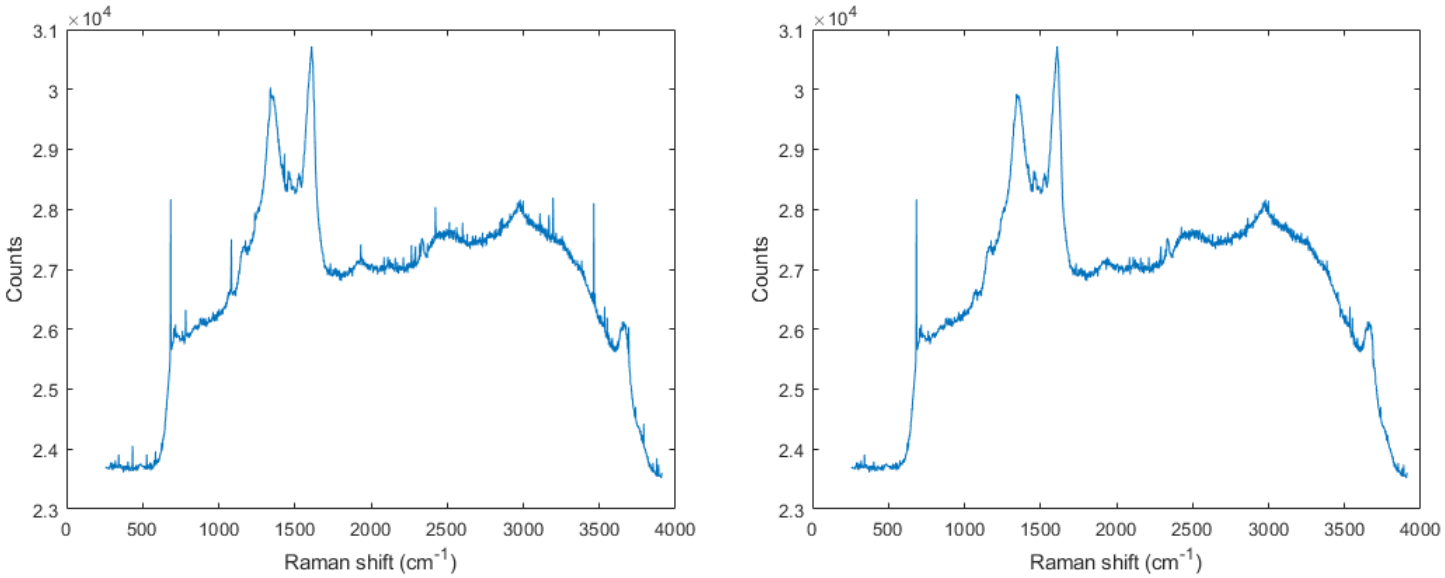

(a) (b)

Figure 13: The Raman spectra of the unheated soot (a) before cosmic ray removal and (b) after cosmic ray removal.

The cosmic rays from the background are also removed and then subtracted from the despiked sample data. It has been observed that the filter also has an influence on the spectrum due to interactions between the laser and filter, acting as a second background for the sample. Hence, the spectrum for the filter is also despiked and the background noise gathered from the filter measurements is removed. After this modification, the filter spectrum is subtracted from the sample by modifying the filter data to match the spectrum. The modification is usually done

with respect to the data around 700 cm^{-1} in the Raman spectrum, though the filter is modified so that it is always below the spectrum in the range 1000-2000 cm^{-1}. Also, the filters should go through the same calibrations and ratio modifications as the sample data has gone through before the removal of the filter, as the filter has the same errors that need to be modified that the sample has. An example of a filter removal is shown in Figure 15. Intensity calibration of the Raman spectrometer is also performed. The known lamp spectrum and the measured spectrum from the setup are shown in Figure 16a, and the intensity calibration ratio is shown in Figure 16b.

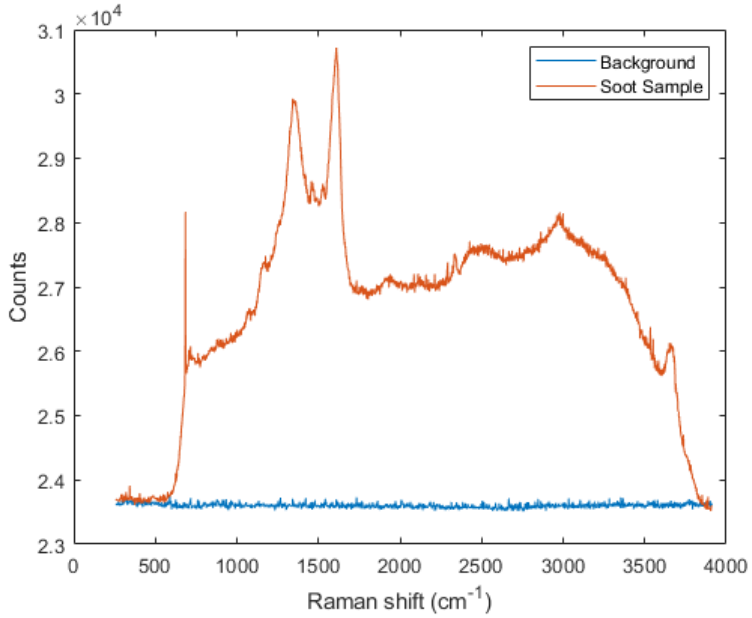

Figure 14: The Raman spectra of a background and a corresponding unheated sample.

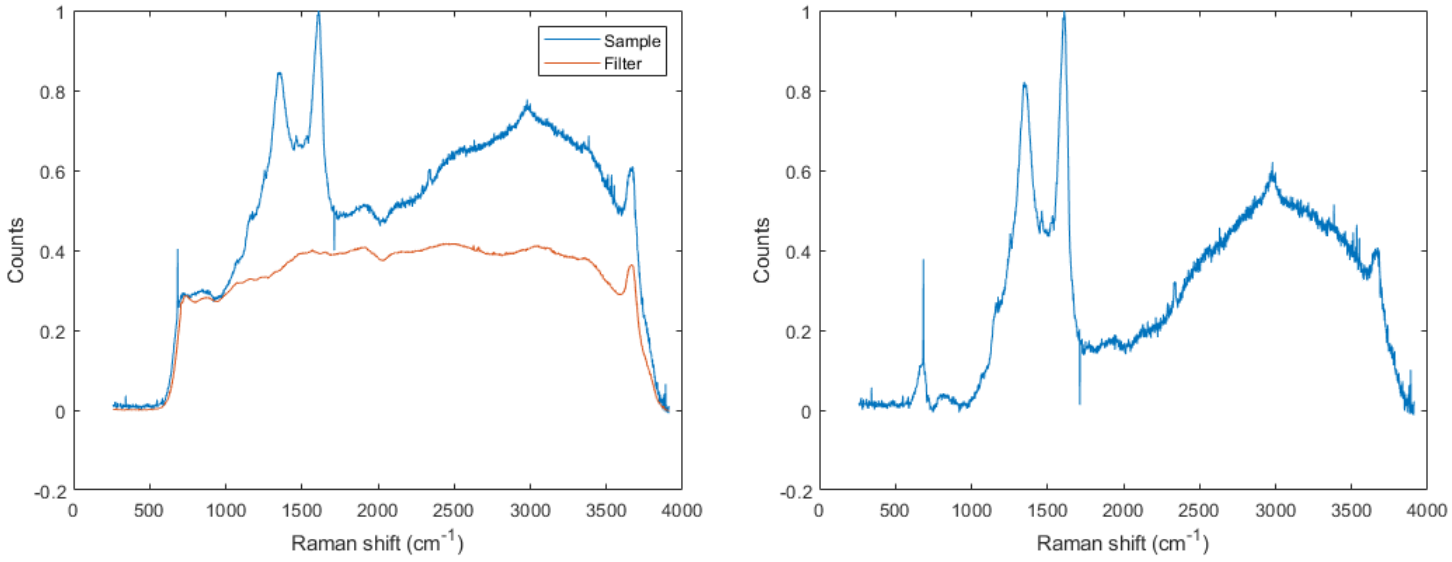

(a) (b)

Figure 15: (a) The Raman spectrum with the filter spectrum. (b) The Raman spectrum with the filter removed.

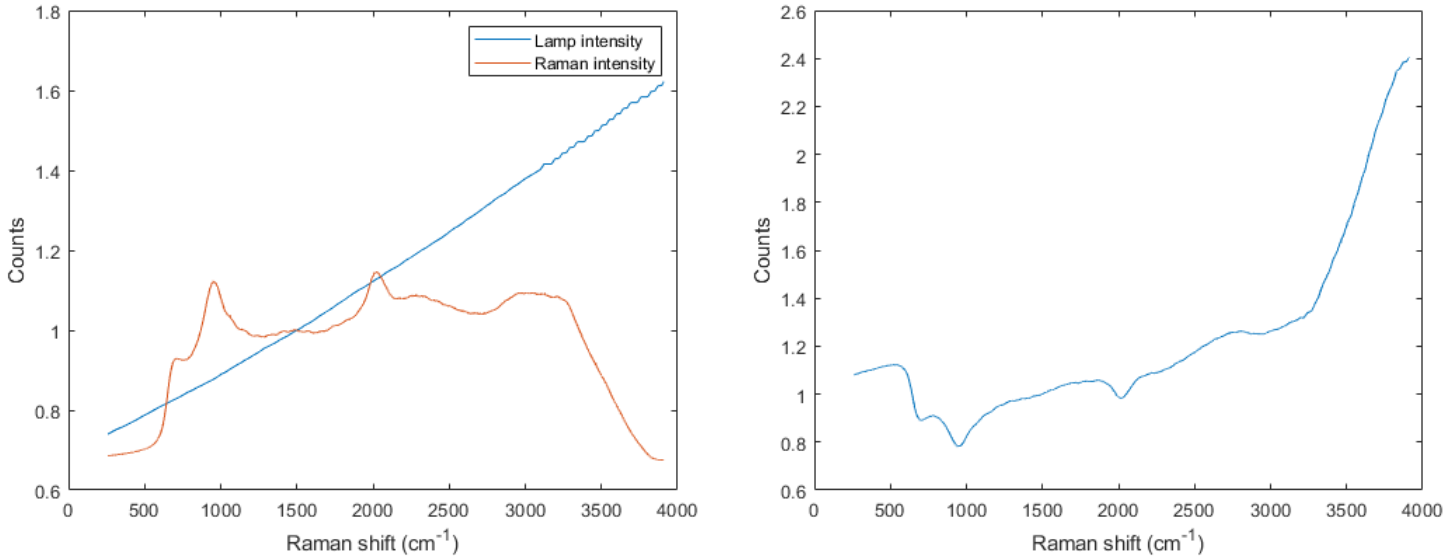

(a) (b)

Figure 16: The intensity calibration. Both spectra are normalised around 1500 cm^{-1}. (a) The measurement and known Raman spectra of a lamp. (b) The ratio between the spectra.

When the above calibrations are done on the Raman spectra, the spectra are normalised around their respective G peaks, after which they are added and averaged. However, the averaging is going to differ depending on the data. The averaging is done either before or after the filter is removed, depending on in which case the spectra look the most similar. If the spectra look equally similar to each other in either case, they are summed and averaged before the filter is removed. This is due to the fact that the removal of the filter can change the positions of the peaks in the Raman shift, so it is preferred to take the sum and average before it is removed. If the spectra were too different from one another, a new measurement would have to be taken so that the poor measurement can be discarded. An example is shown in Figure 17, where the Raman spectra of two unheated soot samples are compared. Both of the samples look similar both before and after the filter is removed, and the filter is therefore removed after the two spectra are summed and averaged, which is the filter removal example shown in Figure 15. The averaged Raman spectrum with a removed filter is normalized with respect to its G peak. This is to make the comparison between the different spectra possible, as the different intensities of the peaks could be due to an overall higher intensity of the data itself.

2.4.2 Deconvolution of Raman spectra

The spectrum is deconvoluted after the normalisation by using the curve-fitting tool from MATLAB. The most important peaks in the Raman spectrum are the 1st order peaks, as those peaks correspond to known structures of the soot. The most important peaks are the D_1 and G peaks, but the D_4 and D'$_1$ are also noticeable peaks around, so the range chosen for deconvolution is 1000-2000 cm^{-1}. This range is chosen because it includes all the important 1st order peaks for the study [6, 14], and gives them enough space to be deconvoluted well, as if a peak is at the edge of the region, there are more difficulties and errors in deconvoluting said peak, as well as leaves enough space for the fit of the fluorescence background to be more accurate.

For the data collected from Raman spectroscopy, the Lorentzian, Gaussian and Breit-Wigner-Fano functions are used to make a curve fit of the data [6]. What functions to use for the curve fit depends on the Raman spectrum. For example, the BWF function is used to deconvolute the G and D_2 peak if at around 1600 cm^{-1} there looks to be a singular peak rather than a curve

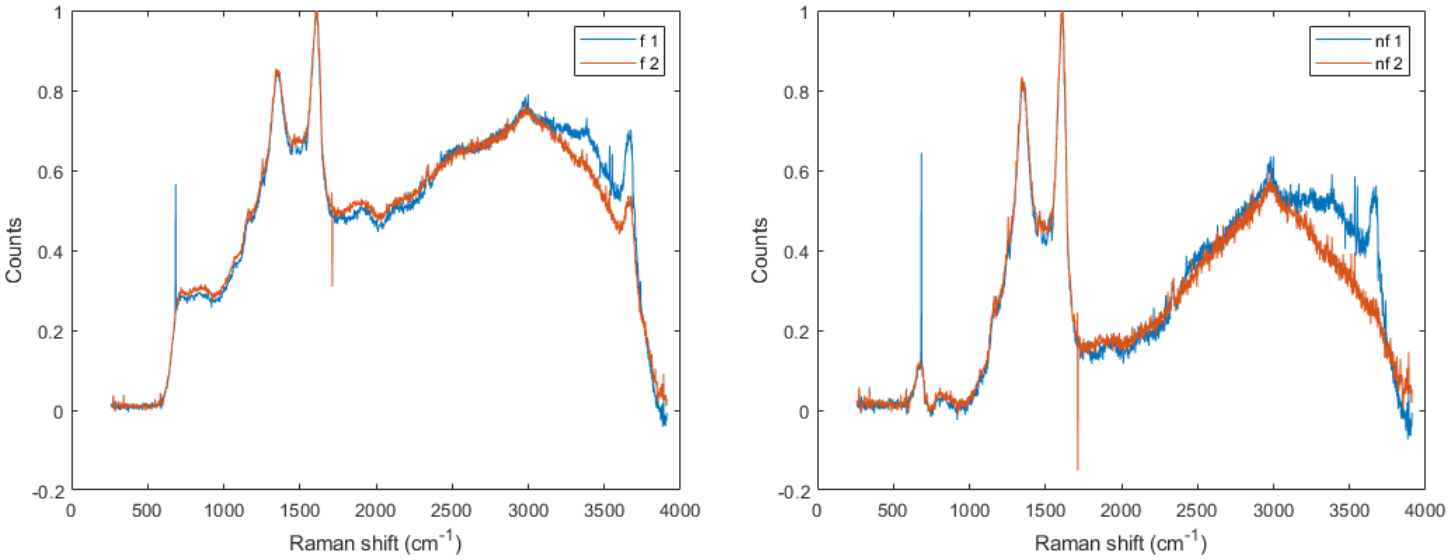

(a) (b)

Figure 17: The Raman spectra of two unheated samples plotted and compared. The samples are normalised around the G peak to make comparisons easier. (a) The samples before the filter is removed. f1 and f2 stands for the first respectively second sample. (b) The samples after the filter is removed. nf1 and nf2 stands for the first respectively second sample.

which can be split into two, or the D_2 peak is not significant in the data [6]. Otherwise G and D_2 are usually deconvoluted by using the Lorentzian function [14]. However, the fitting of D_2 affects the intensity, width and position of G, so it affects important parameters retrieved from the deconvolution. This means that two parameters from two different deconvolution protocols cannot be compared to one another. Therefore one of the methods for deconvolution has to be chosen and used for all the samples. In the majority of the Raman spectra collected, the peak at 1600 cm^{-1} seems to be more like one peak rather than two combined, so the BWF function is used to deconvolute the G and D_2 peak.

In some of the gathered data, there are some noticeable 1st order peaks other than the ones mentioned above. These are described in [6], and the noticeable ones aside from the ones mentioned in Table 1 are, for instance, ether and carbonyl. Taking too many peaks into account for the curve fitting may complicate the curve fitting, so most of these peaks are ignored. However, one peak of these additional 1st order peaks is fitted because it is observed that a more accurate curve fitting is achieved if the curve is taken into account. The extra peak is described in Table 1, which is the C_1 peak. The C_1 curve is fitted with a Gaussian, as the paper which deconvolutes this peak uses a Gaussian function [6]. All of the other peaks are best fitted with a Lorentzian peak, with the exception of D_3, which can be fitted with either a Lorentzian or Gaussian [14]. What function to use for D_3 is not obvious, as it is not noticeable in the graphs and only becomes apparent in the deconvolution. However, one paper, [14], shows that deconvoluting D_3 as a Gaussian curve yields a curve fit which replicates the raw data better. The D_3 peak is therefore fitted as a Gaussian function. A linear function fitted in the range 1000-2000 cm^{-1} and is used to describe the fluorescence background. With this protocol, an example of how a curve fit looks is given in Figure 18a. The fluorescence background is removed from the data, and how the fluorescnece looks compared to the data is shown in Figure 18b. The removal is done to make it easier to see how the deconvoluted peaks and their sums compare to the raw Raman data. The removal also helps for finding the real peak heights of the G and D_1 peaks from the data. The final Raman spectrum with the deconvoluted peaks is shown in Figure 18c.

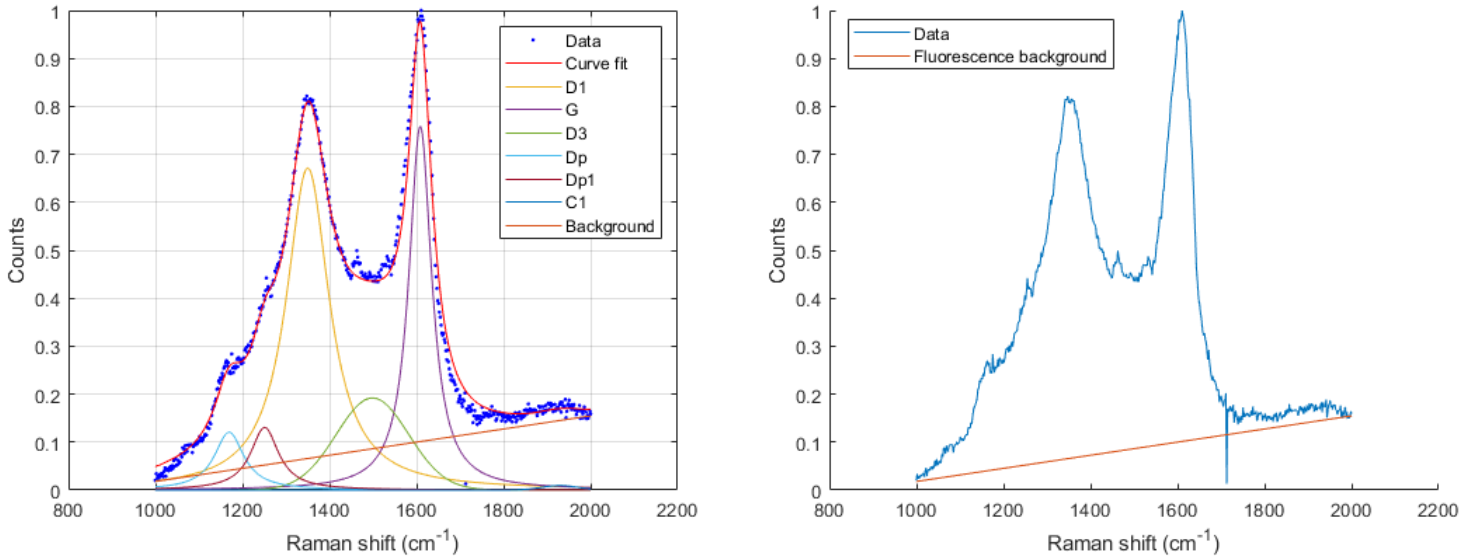

(a)

(b)

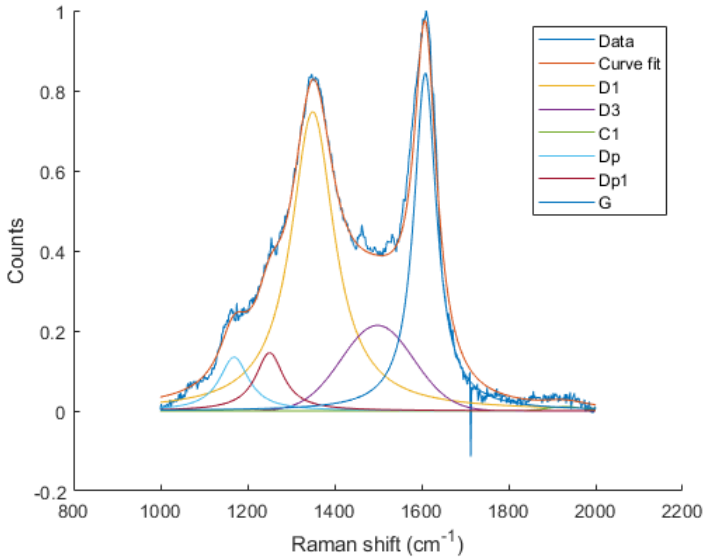

(c)

Figure 18: (a) The deconvoluted spectrum. (b) The spectrum with its fluorescence background. (c) The deconvoluted spectrum with its fluorescence background removed.

Whether a curve is too small or too big can be judged by using that the G and D_1 peaks usually dominate the deconvolution and are therefore close to the data points. However, if one of them is too close to the data, it could mean that some of the other curves are too small. To check that the curve fitting is a good fit for the data, the coefficient of determination, R^2, produced by the curve-fitting tool in MATLAB is used. R^2 is an indication of the goodness of fit of the summed deconvoluted peaks and fluorescence background to the raw Raman spectrum. The curve fit is a better approximation of the data the closer R^2 is to 1, as it shows how proportional the fitted curve is to the data. It should be noted that a R^2 value close to 1 does not necessarily mean a more accurate curve fit for the Raman spectrum, as the good fit could be due to one of the peaks being fitted in an incorrect way, such as the peak being too big or at an incorrect position. Nevertheless, it is attempted to achieve high R^2 values, preferably above 0.99.

A way to analyse the data from the Raman spectrum, which is employed, is with the intensity

ratio between two peaks. The ratios contain information about the soot. The ratios are defined either as the ratio of the peak heights or the peak areas [27]. The peak areas are defined as the integrals of the deconvoluted peaks within the region of deconvolution. The peak area ratio is usually more reliable than the height peak ratio, though there are some cases when the height peak ratio is more reliable [28]. The peak heights can either come from the actual data or the fitted curves, and both these and the peak area ratio are presented. However, it is difficult to judge the height of the peaks in the raw data, other than the G and D_1 peak, so the ratio for the real peak maximums is only taken into account if no other peak is in the ratio. When considering the real height in the raw data, there are also difficulties in finding the actual height of the curves due to the noise of the data. This can be corrected by finding the uncertainty of the spectrum due to noise. This is done by using a region of the data which is relatively flat so that only noise is present and letting MATLAB's function std find the standard deviation. The interval used is between the Raman shifts around 259.8 to 531.4 cm^{-1}. The height of the actual peak is taken as the largest value of the region where G and D_1 are, and then the standard deviation is subtracted from this as the noise makes the peaks a bit higher than they actually are.

The ratios investigated in this paper are I_{D_1}/I_G, I_{D_3}/I_G and m/I_G, where m is the slope of the fluorescence background and the Is are either the area of the peak or height of a peak. These ratios are of interest because they can tell something about the soot. The I_{D_1}/I_G ratio has a correlation with the aromatic layer size of the carbon, denoted as L_a in the literature. This correlation varies, but for soot when $L_a < 2$ nm, the correlation is L_a^2 [27]. Therefore, soot with a higher I_{D_1}/I_G ratio means that the disordered and amorphous carbon are more ordered [29]. The I_{D_3}/I_G ratio gives the amount of amorphous carbon within the soot [30]. The m/I_G ratio is used to measure the bonded hydrogen content, increasing exponentially for increasing hydrogen [31]. Therefore, the logarithm of the ratio is usually plotted. However, some of the fluorescence backgrounds have a negative slope and this will therefore not work for those backgrounds.

2.4.3 Analysis of the results from thermo-optical analysis

The amount of carbon is the area under the carbon curve [18]. The OC, PC and EC can be calculated from this. However, the team who gathered the data has already calculated the total OC and EC, so those values are used to calculate the OC/EC ratio. One can also connect the OC/EC analysis with the ratios for the Raman spectroscopy. For instance, the I_{D_1}/I_G ratio has an inverse relation with the OC content of the soot [29].

This is not the only property that can be found quantitatively from the data. There is also the mass absorption cross-section (MAC). This coefficient can be used to quantify the light absorption [32]. The expression for MAC is [33]

$$\text{MAC} = \ln\left(\frac{T_f}{T_i}\right)\frac{1}{\text{TC}\cdot C\cdot \ln\left(\text{R}(ATN)\right)}, \tag{2}$$

where T_f is the transmission through the clean filter, T_i is the transmission through the filter and soot before the heating. TC is the total carbon measured from the FID signal, C is a correction factor, which accounts for the scatterings by the filter fibers in the clean filter, that has experimentally been determined to be 2.2 [18], and

$$\text{R}(ATN) = \left(\frac{1}{f}-1\right)\frac{\ln(ATN)-\ln(10)}{\ln(50)-\ln(10)}+1, \tag{3}$$

a factor that accounts for the effects from the soot [18]. f is another empirically decided constant

that is 1.6 at wavelength 660 nm [18] and ATN is the attenuation defined as

$$ATN = \ln\left(\frac{I_0}{I}\right), \tag{4}$$

with I_0 being the intensity of the laser while I is the intensity after the laser has passed the loaded filter [34]. The initial intensity is taken as proportional to T_f and the intensity after the loaded filter is taken as proportional to T_i. The actual intensity is a constant multiplied with these transmissions, and this unknown constant is the same for both intensities. It is therefore valid to rewrite ATN as

$$ATN = \ln\left(\frac{T_f}{T_i}\right). \tag{5}$$

The TC needed can be calulcated from the OC and EC values obtained in the OC/EC analysis.

3 Results and Discussion

3.1 Raman data analysis

All ratios are plotted in graphs below. In the graphs, the intensity measured as the area of the peak is marked as A(Peak) and the intensity measured as the height of the peak is denoted as I(Peak). Also, during the discussion of the results, the soot sample with addition of NaCl and KCl are referred to as NaCl and KCl, respectively. The soot sample with no addition of salt is referred to as the reference. From the McKenna burner, the samples are from this point called their HAB. For instance, the sample at 9 mm HAB is just called 9 mm HAB.

For the EC4 step in the KCl, only the first measurement can be used, as all of the soot is evaporated from the second measurement. Only using one measurement gives a higher uncertainty and might give less reliable results compared to the average of two spectra. The evaporation of all soot does not happen with the other samples and might suggest that soot with a KCl additive evaporates quicker than the other samples, and quicker evaporation tends to imply less mature soot [6]. Whether the evaporation actually means less maturity for the KCl is not clear, as the evaporation could be due to some other factor. For all of the samples, the soot from the filter should have evaporated at the EC4 step. This is usually how the heating scheme works, it is to evaporate all soot so the total OC and EC can be calculated. Why there is remaining soot could be because samples with a thicker soot layer than are usually used in the heating protocol are used for the Perkin-Elmer samples during the experiment. This means that the time scales in the heating scheme might be too short to evaporate all of the soot. The thicker layer for the samples is used because an issue during the experiment was that the Raman spectra from the unheated samples with the thinner layer gave results more like the Raman spectra of an empty quartz filter.

Because not all soot is evaporated at EC4, caution should be exercised when reading the results, as the heating steps might not actually represent the changes that would occur if a thinner soot layer was used. Also for EC4, the Raman spectra differed significantly compared to the other spectra of the same sample, implying that the soot is starting to disappear from the filter. It is also supported by the fact that after the heat treatment, there was significantly less soot on the sample. One of the most notable differences between the EC4 spectrum and the other spectra is that the D_4 and D'_1 peaks are not noticeable, and those peaks act a bit odd in the deconvolution due to this, even when allowing those peaks to be zero. The ratios for the EC4 steps might therefore contain more errors, resulting in significant deviations from its actual value. Combine this and that the KCl only had one measurement to work with, the EC4 step is not shown and discussed.

Some R^2 values were below 0.99. In those cases, a different deconvolution protocol could have been used for a better fitting. However, using a different deconvolution method could change

the ratios obtained from the Raman spectrum, so that the ratios can no longer be meaningfully compared with one another. The range of the R^2 value was from 0.9876 to 0.9975.

3.1.1 McKenna samples

For the I_{D_1}/I_G ratio of the McKenna samples (Figure 19), the intensity ratio is increasing with the HAB for the area intensity. This is expected, as the I_{D_1}/I_G ratio for soot is shown to have a positive relation to HAB in other studies [18, 27]. The peak height ratios do not follow this expectation, however. Instead, the sample with a 12 mm HAB is the lowest. This might be because the height for the D_1 peak in the 12 mm HAB differ significantly from the G peak, whereas the heights for the other samples do not differ that much from each other. The reason the area ratio looks better is that the G peak for the 12 mm HAB is very thin, so the area of G is a bit smaller than the other G areas, so it becomes a bit higher.

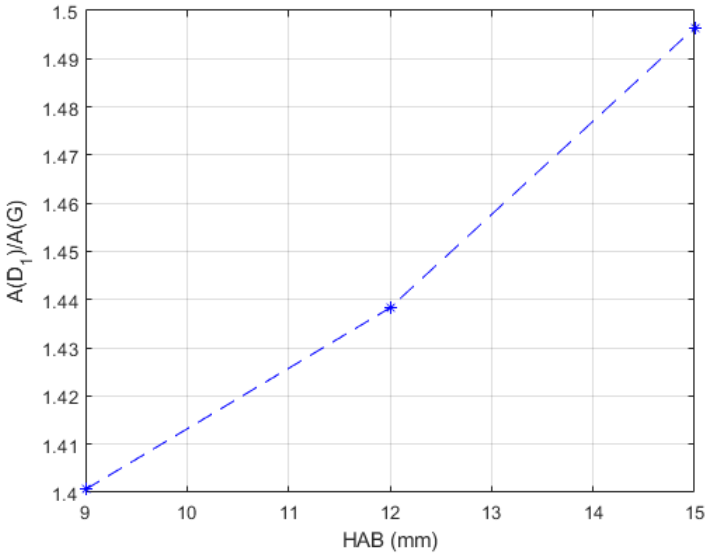

(a)

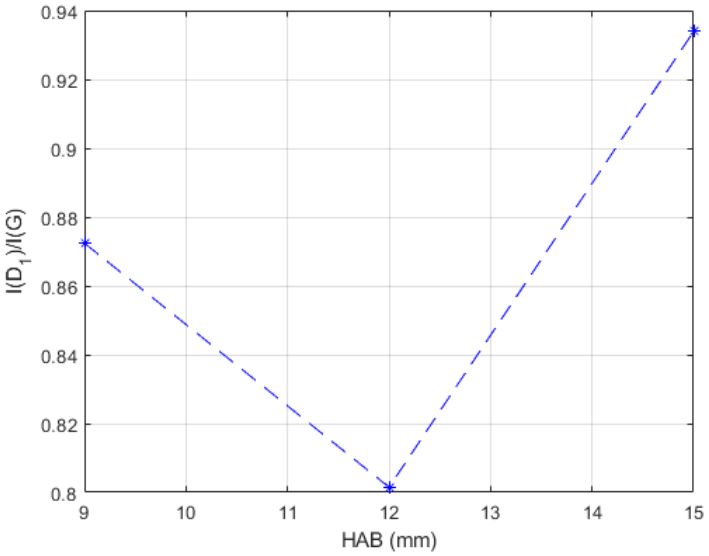

(b)

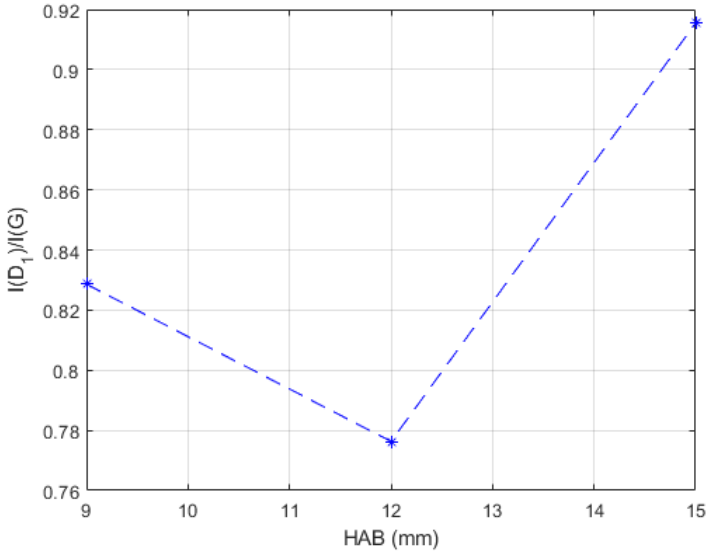

(c)

Figure 19: I_{D_1}/I_G ratio for the McKenna samples. (a) The area ratio. (b) The height ratio from the fitted data. (c) The height ratio from the real height of the peaks.

The I_{D_3}/I_G ratio of the McKenna samples (Figure 20) shows that the 12 mm HAB sample has the highest amorphous carbon, otherwise there seems to be a trend of increasing carbon with HAB. Amorphous carbon is negatively correlated with HAB [35], so the I_{D_3}/I_G ratios obtained here do not agree with previous results. This could be because the ratio for the 9 mm HAB is an outlier, as the expected trend is observed between 12 and 15 mm HAB. However, this cannot be said for certain and is merely speculation.

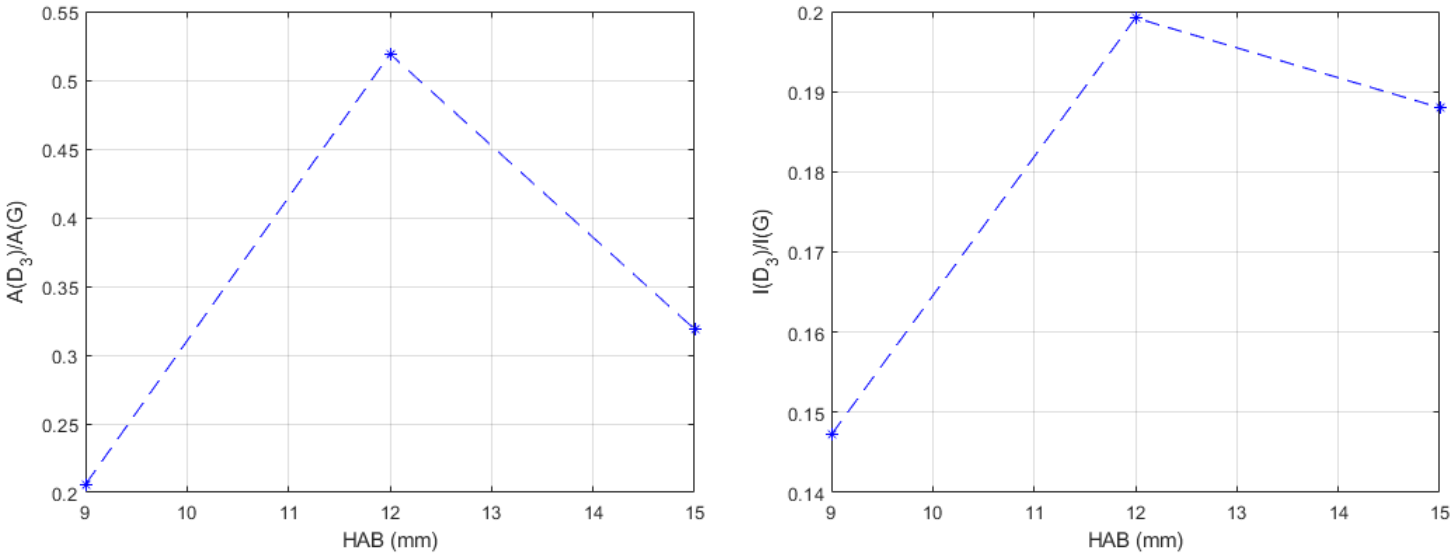

(a) (b)

Figure 20: I_{D_3}/I_G ratio for the McKenna samples. (a) The area ratio. (b) The height ratio from the fitted data.

The $\ln(m/I_G)$ ratio is positively correlated with the OC/EC ratio [18], and, as already mentioned, I_{D_1}/I_G have a negative correlation with OC/EC and a positive relation with HAB, so $\ln(m/I_G)$ should have an negative relation with HAB. In the graphs for $\ln(m/I_G)$ ratio of the McKenna samples (Figure 21), the ratios follow this trend, with the 9 mm or 12 mm HAB being an outlier in the area peak ratio. It can be argued that 12 mm HAB is an outlier for the height peak ratios, as it decreases significantly from the 9 mm HAB, though it can also be argued that the 15 mm is the outlier due to how little it differs from the 12 mm and should actually be lower for the peak height ratios. While it looks like the 12 mm HAB is an outlier in both cases, it is still not easy to judge which sample is an outlier, the results just show that there is one.

Note that for all of the ratios except I_{D_1}/I_G, the height peaks seem to vary less than the area peaks between the different HABs, with the y-axis in the figures having a shorter range for the height ratios compared to the area ratio. This seems to lend support to what is stated in the method, that the area ratio is generally more reliable, though there are exceptions, and seems to be due to being less sensitive to small variations. Small variations could occur due to small errors, and these errors could cause the outliers in the data. Though there must also be another explanation, as most of the significant outliers are in the area ratios. One possible explanation is that the G peak has a small intensity area for the 12 mm HAB compared to the others, as seen in Figure 22. While it is explained by the fact that the G peak in 12 mm is very thin compared to the other samples, it is not very clear why it is so thin. There could be some errors with the results from the McKenna samples in general, as there does not appear to be any obvious relations in Figure 22 between the changes in the spectra and the HAB.

Also, there were some issues with the measurements of the 9 mm HAB, as there are significant differences between their Raman spectra. One of them has a significantly thinner G peak than the other, and due to this significant difference, one of them might be an incorrect measurement.

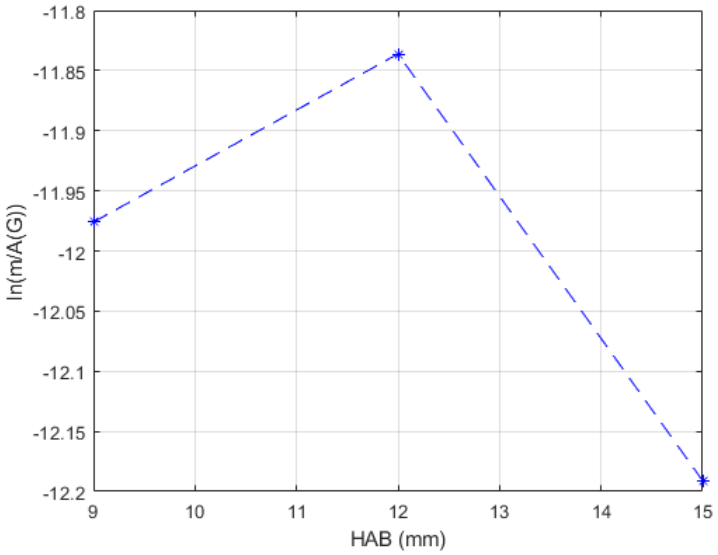

(a)

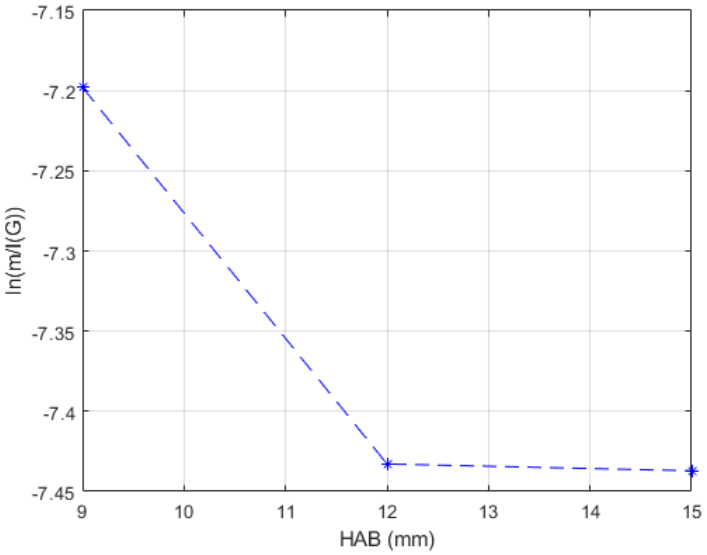

(b)

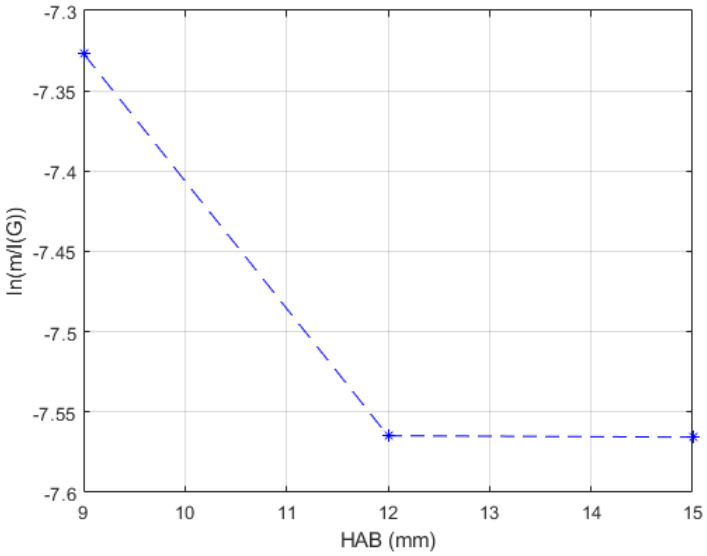

(c)

Figure 21: $\ln(m/I_G)$ ratio for the McKenna samples. (a) The area ratio. (b) The height ratio from the fitted data. (c) The height ratio from the real height of the peaks.

It is not known which is the worse sample, and both of the measurements were used when taking the average. Because of this, it could be the 9 mm HAB which is an outlier rather than the 12 mm HAB. The fact that one bad measurement is found and it is not known which one is bad and should not be discarded, shows the limitation of just using two measurements in the average. This could be fixed by taking an additional measurement. The only sample which had two significantly different measurements after modifications was the 9 mm HAB, so it is not a problem for the other samples.

Also, the techniques for finding the ratios seem to be sensitive, as at least one outlier is retrieved from some of the ratios. This is supported by an observation during one deconvolution, where it was observed that two good curve fits on the same graph can give very large differences in the I_{D_1}/I_G area ratio, at one point ranging between 1.2-1.6. One reason for this could be that the area ratio depends on both the height of the deconvoluted curve as well as its thickness.

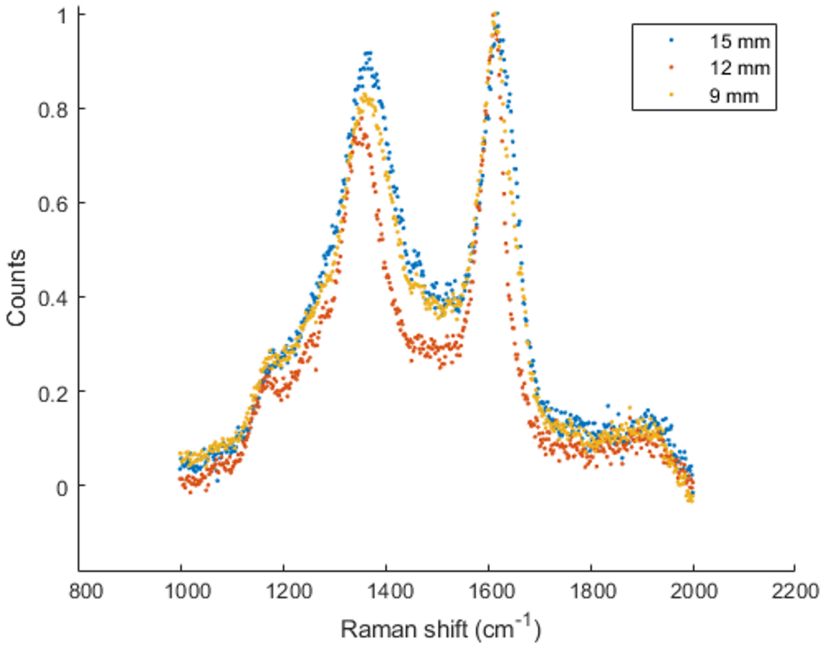

Figure 22: The Raman spectra of the unheated McKenna samples after modifications. The fluorescence background is removed.

While the interval which is integrated to obtain the area intensity of a curve is generally such that the whole Lorentzian/Gaussian peak is integrated, the peak is modified with a multiplication of the peak and a constant to make the peak fit the data. This constant can modify a thick peak to have the same height as a thin peak, resulting in a larger area due to the peak being thicker. Due to both parameters influencing the area, the area ratio can also be considered sensitive.

3.1.2 Perkin-Elmer samples

While the different methods for the ratios give different results for the Perkin-Elmer soot, as in the McKenna samples, there still exist some consistencies between them. For the I_{D_1}/I_G ratio (Figure 23), before any heating is done, the ratios are lower for the KCl and NaCl compared to the reference. This indicates that the salt causes more disorder in the soot prior to the heat treatment. This might be intuitive, as the salts come with more chemicals not usually found in soot, and might increase the probability that the new chemicals bind to the carbon to create more OC or that the structure of the soot is disrupted by the salts. The I_{D_1}/I_G ratios for the NaCl are always lower than the reference at any given step, so it always has more disorder than the reference. This might be due to the samples changing in a similar manner during the heating, though with some outliers. The fact that NaCl seems to increase/decrease similarly to the reference might hint that the addition of NaCl into the sample does not affect how the order of the soot changes during the heating scheme. During heating, the I_{D_1}/I_G for the KCl is always larger than NaCl. This indicates that the KCl and NaCl act differently during heating, though it might be due to the sudden increase for KCl at OC1, with the exception of the real peak ratio, where it decreases very slightly instead, that causes KCl to be above NaCl. The KCl and NaCl both look like they follow a similar rate of increase and decrease for all of the ratios, especially during the heating, and these results suggest that there is no significant difference between the different salts in how the order of the soot sample changes when it is heated in different environments.

How the ratios increase/decrease is not consistent between the different techniques. The peak height ratios both follow a similar general pattern, the samples first decrease and then

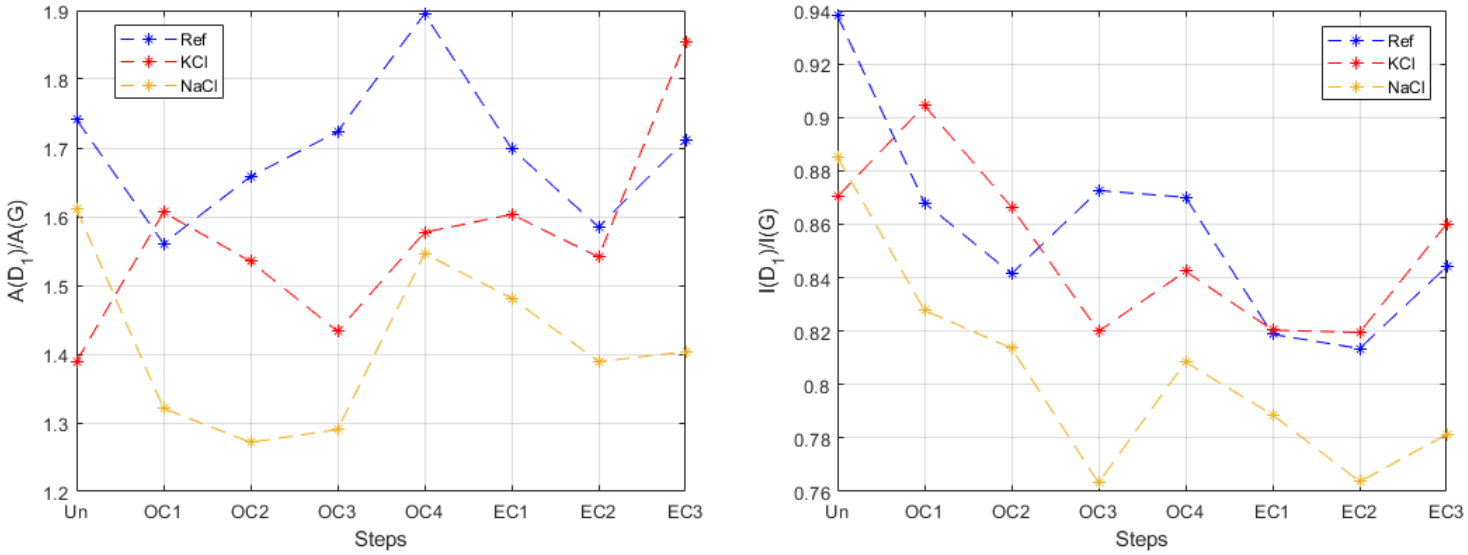

(a) (b)

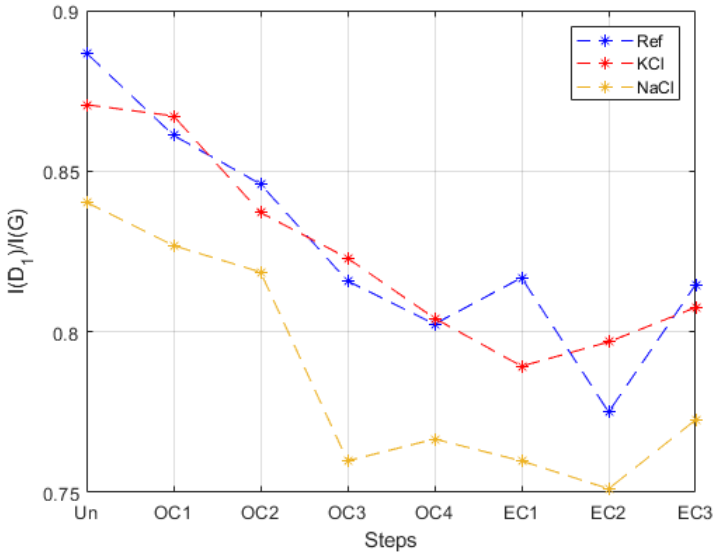

(c)

Figure 23: The evolution of the I_{D_1}/I_G ratio for the Perkin-Elmer samples during heat treatment. (a) The area ratio. (b) The height ratio from the fitted data. (c) The height ratio from the real height of the peaks.

increase the ratio as it moves along the steps. The NaCl and reference both starts increasing more consistently after EC2 and the KCl seems to start increasing earlier, after EC1. For the area ratio, however, the reference generally increases up to OC4, where it decreases afterwards to then increase at EC3. The NaCl follow a similar pattern, except that it decreases for all steps before OC3. The KCl seems to follow the general pattern of decreasing before it increases at OC4, where it then overall increases. The KCl and reference both follow similar curves for the peak height ratios, but not for the area ratio. Instead, the reference's ratio increases in the interval OC2 to OC4.

It is noticeable that some of the ratios increase at the OC4 step, which agrees with Ess et al. [29], where it was found that the ratio increases after 400°C. However, the heating in [29] is done in pure air, meaning the oxygen occupies approximately 21% of the environment, whereas in

this paper the heating is done in an environment with oxygen ranging from 0% to 2%. A rough approximation of air is to say that it consists entirely of nitrogen, but this approximation may not work here due to the significantly different oxygen between the two environments. Looking at the results from Le et al. [6] used pure N_2 during heating and the authors report similar results as [29]. This might imply that while the environments do play a part in how the Raman spectrum evolves with heating, some other factor might have a more significant influence.

The OC3 step is at 450°C, so the change of the ratios from this study are not entirely consistent with [29], which might be because the authors of the study held the temperatures at 15 minutes, which is significantly longer than the times the temperatures are held at in this paper. The longer heating time could result in more significant changes in the soot. However, [6] reported similar results, and the temperature was held for 1 minute, which is more like the time at which the temperatures are held in this paper. However, [6] takes smaller heating steps, so it can influence how much the sample is heated before it reaches the temperatures used in this paper's methods. Hence, while the results agree to some extent with [6] and [29], the different times held at the temperatures along with the number of steps taken can result in the ratios changing differently compared to the results presented here. Also, due to [6] and [29] using different steps, times and environments from each other, it may be hard to compare their results and from that conclude what causes the results from this project to differ from theirs.

For similarities between all of the I_{D_3}/I_G ratios (Figure 24), the ratios for the KCl and NaCl are bigger in both ratio techniques before any heating is done, indicating that the KCl and NaCl have more amorphous carbon. This result aligns with [13], which found that the I_{D_3}/I_G was higher for soot with KCl. The presence of amorphous carbon implies that some of the structure within the soot is disordered. This aligns with the discussion above where it is suggested that the salt causes some disorder in the soot. The KCl follow a similar change as the reference for both ratios, though the rate of the increase/decrease can differ significantly, as seen in the area ratio at step OC3. The significantly different rate of the change might be an outlier, as it is not observed on the same step in the peak ratio. This implies that KCl does not affect the change of the amorphous carbon when the sample goes through a heating procedure.

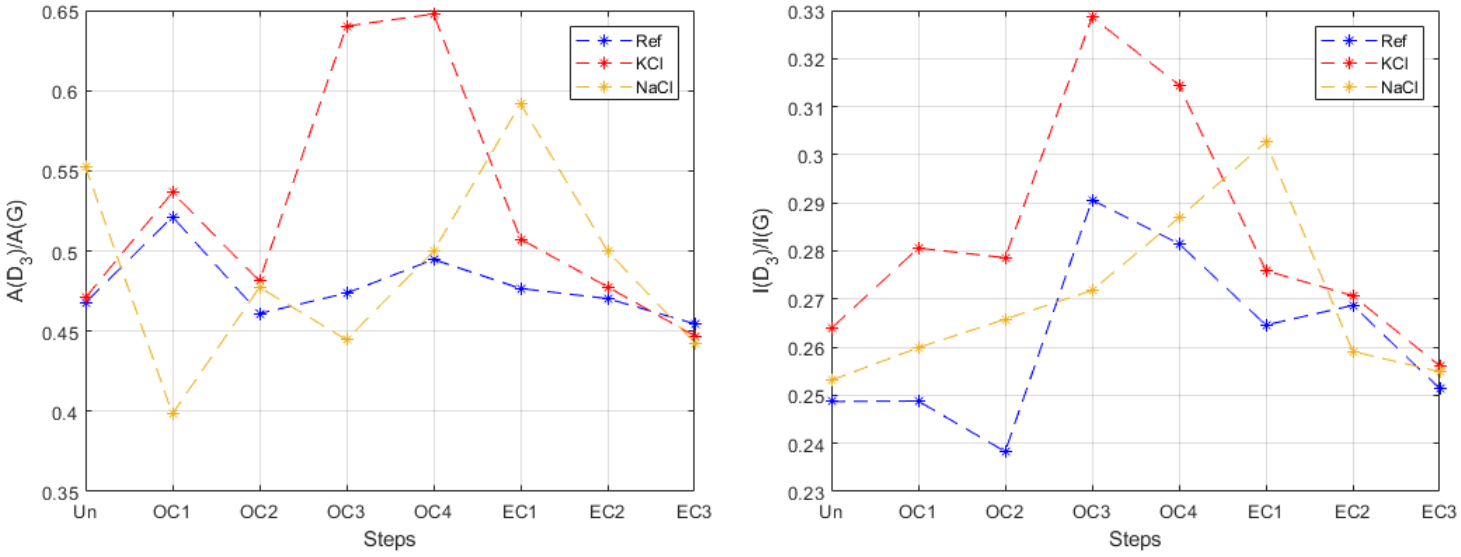

(a) (b)

Figure 24: The evolution of the I_{D_3}/I_G ratio for the Perkin-Elmer samples during heat treatment. (a) The area ratio. (b) The height ratio from the fitted data.

For the area ratio, the KCl and reference generally increase until EC1, where they decrease. For the peak ratio, both samples start decreasing at OC4. For the NaCl, the area ratio changes

unpredictably at the start, but it starts increasing consistently after OC3, and it starts decreasing at EC2. The peak ratio for NaCl shows a more consistent increase until EC2, where it decreases. The NaCl follows a similar general pattern of first increasing and then decreasing. This is the opposite pattern as the I_{D_1}/I_G ratios, which is expected as stated in the discussion of the I_{D_3}/I_G in the McKenna samples.

The heating step where the NaCl starts to decrease is shifted towards a later heating step compared to the other samples. Amorphous carbon causes some disorder in the soot, as amorphous carbon per definition lacks local order [6], so the fact that NaCl decreases at a later heating step means that it will not become more ordered until it has reached a higher temperature or a change in the environment in which the sample is heated. For the area ratio, the decrease for the samples does not happen until air is added into the environment, though the temperature exposures beforehand could also cause the loss of the amorphous carbon during the EC steps. It is therefore uncertain whether the change is due to the temperature increase, environmental change, or both.

Because the $\ln(m/I_G)$ ratio is not valid for all the slopes obtained in the deconvolution, as some of them are negative, the regular m/I_G ratios are plotted instead, and are shown in Figure 25. The different methods for finding the m/I_G ratio give similar outcomes, with the biggest difference being the scale on the y-axis in the graphs. The fact that the ratios do not differ too much between the different techniques is not too surprising, as the slope m can only be measured one way and is therefore the same for all ratio techniques. The only difference is the I_G that m is divided with, and the area and both peak heights have a positive correlation with each other. Interestingly, the m/I_G starts off as lower for both KCl and NaCl, with the ratio for the KCl being the lowest. This implies overall lower bound hydrogen content in the KCl and NaCl before any heat treatment. This could be due to the salt affecting the hydrogen or how well it is bounded to the carbon, which could be because the salt causes the hydrogen bonds to break up. One study found that hydrogen bonds break up with the addition of salt in water-ethanol mixtures [36], and the fuel used in this project for the creation of the soot samples is similar to ethanol (C_2H_6O) in chemical composition. It is therefore possible that the lower bound hydrogen in the KCl and NaCl comes from the break of hydrogen bonds. After around OC1 or OC2, the reference starts to have lower bound hydrogen than NaCl and remains lower than NaCl for the other heating steps, with the exception of EC3. The reference also has lower bound hydrogen content than KCl between the steps OC3 and EC2. The KCl is always lower than NaCl, with the exception of the OC3 step, implying that less bonded hydrogen forms with the addition of KCl.

All of the samples follow a similar pattern, their ratios first decrease for the heating steps and then increase, except I_{D_3}/I_G which has the opposite pattern. The decrease is expected, as the bound hydrogen content has a positive correlation with the OC of the sample [18], and the first steps are to remove the OC. The increase can be due to other carbons being evaporated, making the relative hydrogen content of the sample larger. This can happen when the heating protocol is at the EC steps. This is supported by looking at the KCl and NaCl in the graphs in Figure 25, as they do not experience an increase in their ratios until EC1 and EC2, for KCl respectively NaCl. The graphs in Figure 25 also show that the reference starts to increase at OC4, which could be due to the ratio at OC3 being a bit lower than it should be, and the reference therefore does not experience an increase until later, though this is just speculation. It might also be that the higher temperature causes other OCs in the soot to evaporate more, causing the relative hydrogen content to increase. The fact that when the increase happens is shifted for the different samples implies that the addition of any of the salts affects when the ratio starts to increase. Though because the ratios are so small, they are sensitive to errors, and there might not actually be a shift for the increase.

Also, the NaCl seems to first follow a similar change as the reference, but around OC3 to EC2, it follows a similar curve as the KCl. The rate at which the ratio changes for the different

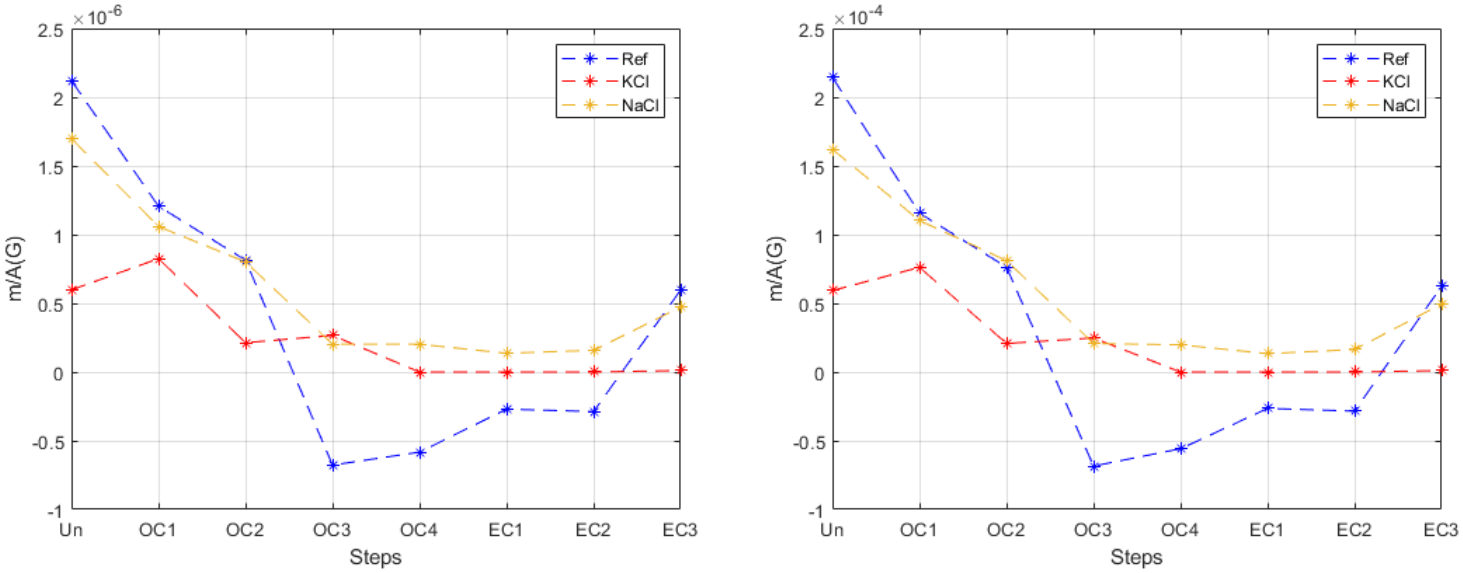

(a)

(b)

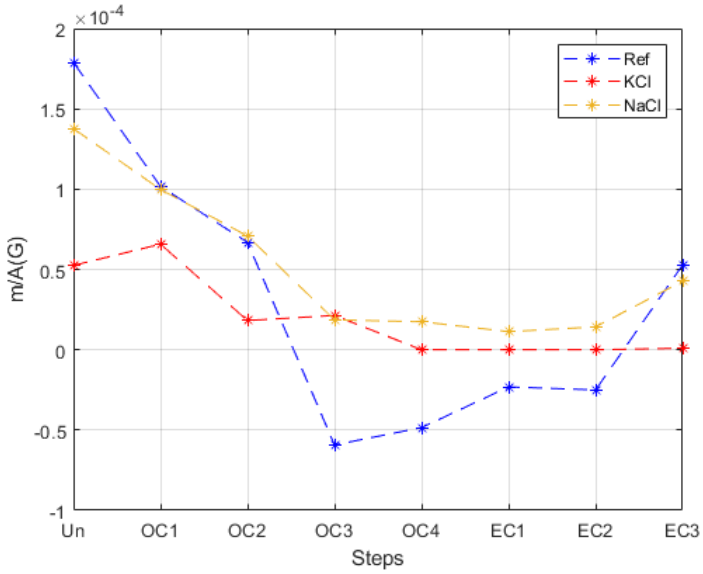

(c)

Figure 25: The evolution of the m/I_G ratio for the Perkin-Elmer samples during heat treatment. (a) The area ratio. (b) The height ratio from the fitted data. (c) The height ratio from the real height of the peaks.

samples could be due to the salts, and because the NaCl follows the reference curve at some steps might mean that the KCl affects the rate of the change more. Comparing the I_{D_3}/I_G ratios with the m/I_G ratios, I_{D_3}/I_G tends to increase in regions where m/I_G decreases, and vice versa. This is in agreement with [29], which found that the amorphous carbon has an inverse relation with the OC content of the sample. This could also explain why the hydrogen content is initially lower for the KCl and NaCl, as they initially have more amorphous carbon. The results for the m/I_G ratios also agree with those found in [15], which shows that m/I_G decreases when heated in air up to 500°C, especially for less mature soot. While [15] does not show what happens at higher temperatures, why an increase could happen is already discussed above.

Figure 26 shows the Raman spectra of the unheated Perkin-Elmer samples. There are some notable but subtle differences, such as the D_1 peak and the 1500 cm^{-1} region having a

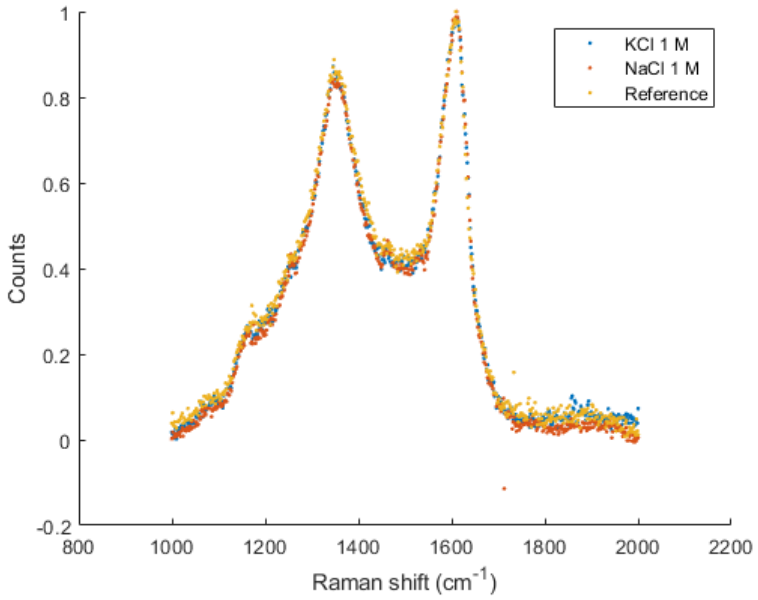

Figure 26: The Raman spectra of the unheated Perkin-Elmer samples after modifications. The fluorescence background is removed.

slightly different height, and the 1800-2000 cm^{-1} region seems to vary a bit between the samples. However, the spectra are overall similar to each other. This is reasonable, as the spectra shown are characteristic for soot, so they should not differ significantly from one another. The D_1 peak appears to be a bit larger for the reference, which agrees with the I_{D_1}/I_G ratio. Interestingly, the 1500 cm^{-1} region seems to have a higher height for the reference compared to the other samples, even though the I_{D_3}/I_G ratio is smaller for the reference.

Interestingly, the change in the G peak seems to be very small compared to the other changes. This could be due to the normalisation being with respect to the G peak, but even the width is relatively unchanged. This is in contrast to the McKenna samples in Figure 22, where the G peaks have noticeably different widths. This seems to lend support to the discussion that there are outliers in the McKenna samples that give the unexpected results, and the samples from the Perkin-Elmer might therefore provide more reliable results. Another reason the Perkin-Elmer samples have more similar Raman spectra to each other compared to the McKenna samples might be because the change of the HAB has a stronger influence on the soot than the addition of salts. The salt concentration used for the KCl and NaCl samples are low, around 700 ppm, so the influence of the salts used could be low too. However, due to the flaws in the results from McKenna samples, it is hard to verify from the results if if HAB actually has a stronger influence in this case.

Comparing the Raman spectra for the different heating steps (Figure 27), the spectra do not differ much from each other, and the noticeable differences are the same as between the different samples. It seems that a decrease in the heights of the D_1 and D_4 peaks, and an increase in the height of the 1500 cm^{-1} region occur with increasing temperature. This should be interpreted with caution, as some of the points overlap with each other and some points are therefore hard to see in the graph. This means that some increase or decrease between the steps could happen that contradict the overall relation, but is not visible in the graph. Still, an overall decrease of the D_1 peak is consistent with the results from the I_{D_1}/I_G ratios of the steps, though there is always an increase in the ratio at the end of the heating scheme. Looking at Figure 27, it seems that EC2 is smaller than EC3 for all samples, which also agrees with the I_{D_1}/I_G ratios, as seen in Figure 23. The fact that the 1500 cm^{-1} region seems to have an opposite change with temperature compared to the D_1 peak agrees with the results of the I_{D_3}/I_G ratios, as their

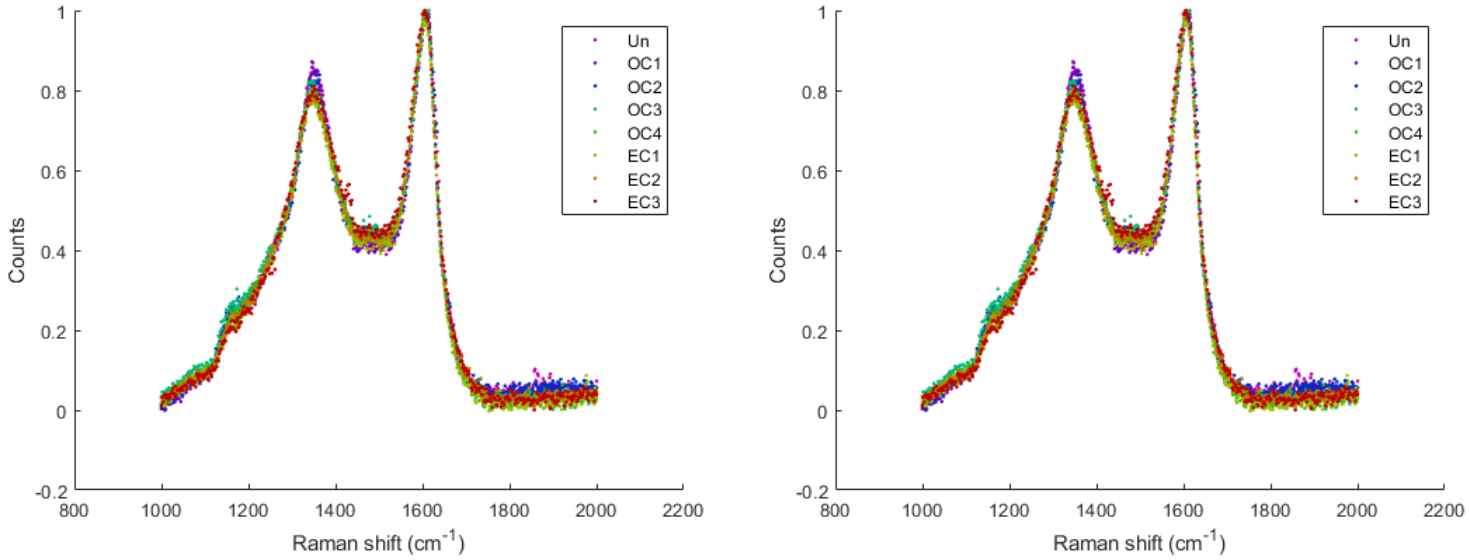

(a) (b)

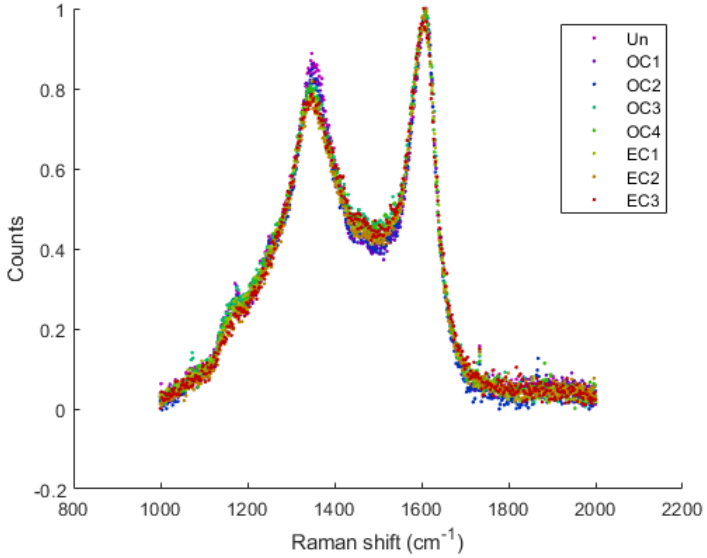

(c)

Figure 27: The Raman spectra for the different heating steps after modifications. (a) The KCl. (b) The NaCl. (c) The reference.

change with temperature was also the opposite of that of I_{D_1}/I_G. The decrease in D_4 agrees with [29].

The lid removed / lid on ratio is flawed in this study, as the background was not removed. It should have been removed due to the fact that the presence or absence of the lid does not affect the background. However, removing the background would cause some of the points to be close to zero, potentially causing some of the values in the ratio to go to infinity. The points in the Raman spectra where the ratio becomes large are outside the range used, so it could have been used without much concern. The fact that the background should be removed was noticed too late and is therefore not corrected for. This error means that the data could be modified such that the results are incorrect. However, it was found that removing the background did not have such a big impact on the samples when the data was normalised with respect to the G peak, so the errors, if there are any, are probably insignificant.

3.2 Thermo-optical analysis

3.2.1 OC/EC analysis

The OC/EC ratio for the samples are given in Table 3. The HAB of the McKenna samples have a negative correlation with the OC/EC ratio, which is the expected result as a higher I_{D_1}/I_G ratio, which is positively correlation with HAB, implies lower OC [29]. The OC/EC for the reference from the Perkin-Elmer burner is significantly lower than the McKenna sample at 15 mm HAB, which is not too unexpected as while the HAB is lower for the Perkin-Elmer burner, the fuel mixture is different between the two burners too. The composition of the fuel has an influence on the soot formation process [3], which in turn could cause a difference between the OC/EC ratio. This means that the OC/EC ratios cannot be easily compared between the different burners. In fact, flames that are rich in fuels, or have a higher equivalence ratio, tend to give more OC [29], and tend to therefore be less mature. However, the Perkin-Elmer burner had a larger equivalence ratio than the McKenna burner (though there may be more carbon available for the soot formation for $\Phi = 2.6$ than $\Phi = 2.1$), so there is probably some other properties of the burners, that influence the OC and EC composition.

Table 3: The OC/EC ratio and MAC for the soot samples. The length given for the McKenna samples is the HAB for that sample.

Soot sample	OC/EC	MAC (m^2/g)
Perkin-Elmer reference	0.17	8.3
Perkin-Elmer NaCl 1M	0.27	7.8
Perkin-Elmer KCl 1M	0.52	6.1
McKenna 15 mm	0.51	2.8
McKenna 12 mm	1.7	2.0
McKenna 9 mm	3.9	1.0

Comparing the Perkin-Elmer samples, the reference has the lowest OC/EC ratio and the KCl has the highest. This is an interesting result in reference to the results from the $\ln(m/I_G)$ ratios, which imply that the hydrogen content is lower for the KCl and NaCl before the heating, so it seems like two results are obtained that contradict one another. However, metal salts in general, which includes alkali salts, have been shown to affect the OC/EC ratio due to acting as a catalyst that enhances charring of OC and/or reduces the oxidation temperature of EC [37]. This can interfere with the pyrolysis correction [37]. Another reason could be that the addition of KCl and NaCl has been shown to decrease the size of soot particles [12], and as the soot particles mature they grow and become carbonized [4]. Hence, KCl and NaCl could interfere with the maturation process of soot particles, causing less EC to be formed. It has also been found that KCl has the largest influence on the particle size [12], so the larger OC/EC for KCl agrees with previous results.

There is some uncertainty when calculating OC and EC [18, 29, 38]. The uncertainty stems from the correction for PC, with the correction working under the assumptions that PC is similar to EC and evolves before EC [18]. These assumptions are not always correct [38], which causes the uncertainty to still be a problem. This uncertainty causes the OC/EC ratio to be very sensitive. Therefore, small differences between the OC/EC of different samples cannot be seen as meaningful. The OC/EC for the reference and KCl soot differ significantly enough to not be considered a problem, but the difference between the reference and NaCl is a bit small. Though the results from the Raman spectroscopy experiment does show that NaCl acts more like a less mature sample compared to the reference, so the results for the OC/EC might be accurate. Though the m/I_G ratio does imply that KCl and NaCl are more mature than the

reference, but the other Raman peak ratios indicate that KCl and NaCl are less mature. It is interesting that the OC/EC between the McKenna 12 and 9 mm HAB follow the expected OC/EC relation, with the 9 mm HAB being the largest. This implies that there was something with the measurement or some local variation that causes the unusual results from the Raman spectra.

3.2.2 Mass absorption cross-section

For the MAC, studies have shown that it has a negative correlation with OC/TC [18, 32, 33]. If MAC has a negative correlation with OC/TC, it also has a negative correlation with OC/EC, as TC = OC + EC, so OC/TC can be rewritten as $1/(1 + \mathrm{EC/OC})$, which decreases as EC/OC increases, and EC/OC has a negative correlation with OC/EC. The McKenna samples follow this correlation, as seen in Table 3. This indicates that MAC is a decently reliable parameter for analysing the absorption efficiency of the soot. The MAC for the Perkin-Elmer samples also shows consistent decrease for the KCl and NaCl samples, with the KCl having the smallest MAC. This is the expected result, as the KCl has the largest OC/EC out of the Perkin-Elmer samples. The result also agrees with previous research that showed that the addition of NaCl and KCl reduced the light absorption coefficient [3, 12, 13, 30].

All of the MACs follow the expected relation with respect to their OC/EC, except for the KCl and 15 mm HAB. Their OC/EC are almost the same, but their MAC differ significantly. Why this is the case is not known, though one speculation is that the MAC is calculated incorrectly and gives incorrect values. It is assumed that the same f value is valid for all MACs, even though Weingartner et al. [34] shows that f differs for different soot. An incorrect f might therefore be used, which gives incorrect estimates of MAC. In fact, from [34], the f for fresh soot samples with transmission wavelength 660 nm is reported to vary between 1.34 and 1.89. This variation means that the values for the R(ATN) can differ quite significantly, though it may not be significant enough to give noticeably different relations to the MAC.

3.3 OC/EC and Raman peak ratios comparison

For soot, the I_{D_1}/I_G ratio has been shown to be bigger for lower OC/EC ratio [18, 29]. This correlation might be because both parameters have the opposite relation to the soot's maturity, as stated above. Comparing the OC/EC ratios with the I_{D_1}/I_G ratios for the unheated samples in Figure 28, the ratios seem to follow this relation, with the exception of a few outliers. Specifically, the NaCl has the lowest real height ratio of the Perkin-Elmer burner. All OC/EC ratios from the Perkin-Elmer burner are higher than the OC/EC for 15 mm HAB, while all unheated Perkin-Elmer samples' area I_{D_1}/I_G ratios, except the KCl, are larger than the I_{D_1}/I_G from the McKenna samples. While comparisons might not be useful between burners due to differences in the flames of the burners, as mentioned above, it is still interesting that the MACs from the Perkin-Elmer samples implied that the Perkin-Elmer samples are more mature overall compared to the McKenna samples. The area ratios for the Perkin-Elmer samples also imply more maturity. This only applies for the area ratio, however, and the other Perkin-Elmer samples' I_{D_1}/I_G are below the I_{D_1}/I_G for the 15 mm HAB, except the reference's ratio for the fitted height ratio. The height I_{D_1}/I_Gs in the McKenna case are considered to be slightly flawed, for reasons already discussed.

The relation between the I_{D_3}/I_G and OC/EC ratio is not as clear from the literature. Liu and colleagues [35] showed that I_{D_3}/I_G decreases with increasing HAB, implying that the amorphous carbon increases with increasing OC/EC. However, Ess et al. [29] reported that the amorphous parts of the soot decreases with increasing OC. Both are valid, as amorphous carbon could be either OC or EC, depending on if it is regular amorphous carbon or hydrogenated amorphous carbon [4], and amorphous carbon generally imply more disorder, causing a negative correlation between I_{D_3}/I_G and I_{D_1}/I_G. These mixed results means that it is not exactly known how I_{D_3}/I_G

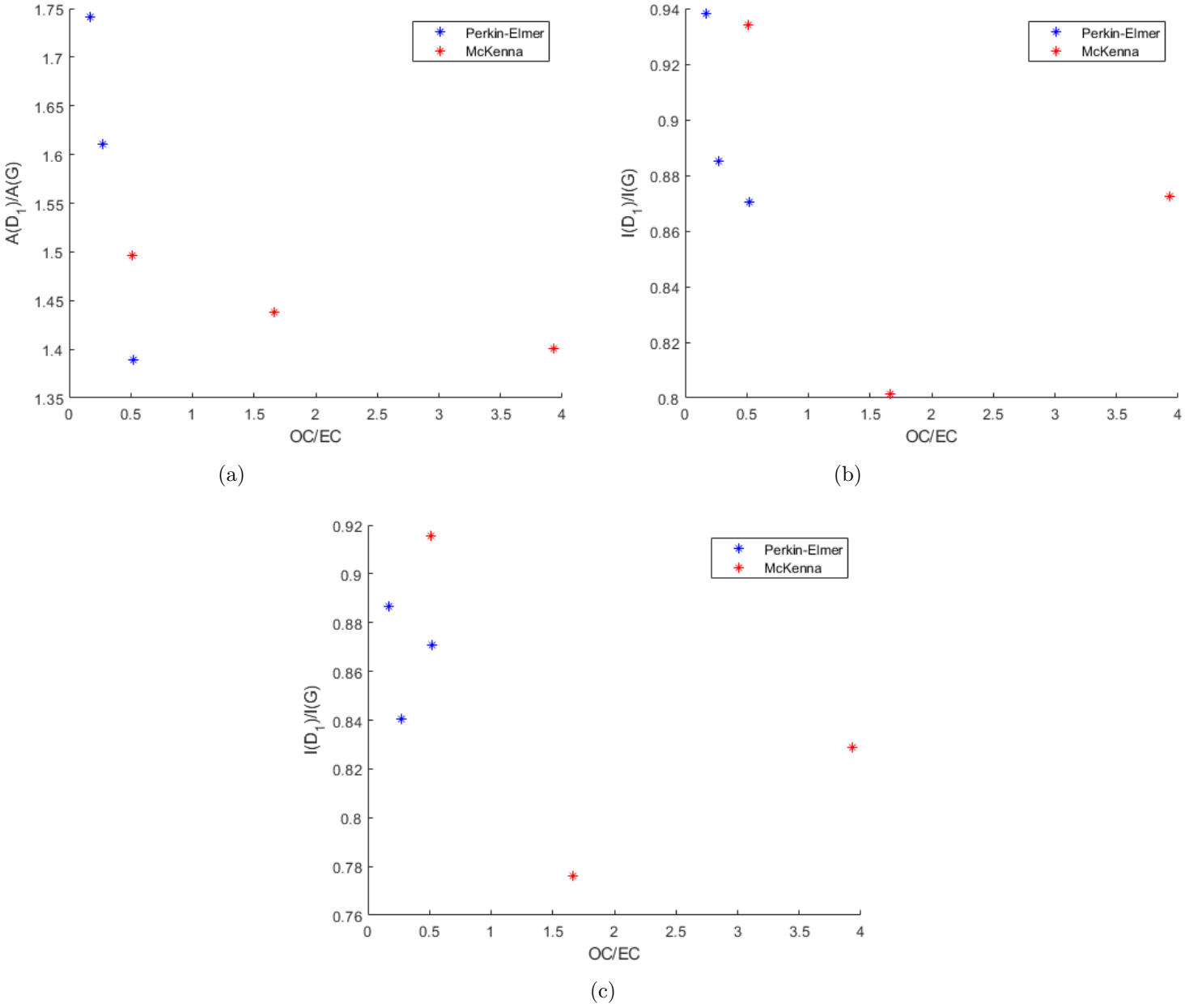

Figure 28: I_{D_1}/I_G plotted as a function of OC/EC. (a) The area ratio. (b) The height ratio from the fitted data. (c) The height ratio from the real height of the peaks.

would relate to the OC/EC. Comparing the I_{D_3}/I_G of the unheated samples with OC/EC in Figure 29, the results are hard to interpret due to the mixed results, especially from the McKenna samples. In general, the unheated Perkin-Elmer samples have larger I_{D_3}/I_G than the McKenna samples. This generally means more amorphous carbon in the Perkin-Elmer samples, and could imply that amorphous carbon decreases with increasing OC/EC.

As stated above, the $\ln(m/I_G)$ ratio is positively correlated with the organic content. The positive correlation between OC/EC and $\ln(m/I_G)$ is therefore reasonable, as $\ln(m/I_G)$ represents the bound hydrogen content in the soot and hydrogen bound to carbon would create some type of OC. Comparing the ratios (Figure 30), it is seen that the McKenna samples follow the relation, as overall the soot generated at a lower HAB has a higher $\ln(m/I_G)$ ratio compared to higher HABs. The $\ln(m/I_G)$ ratios from the McKenna samples are overall higher than the ratios obtained from the unheated Perkin-Elmer samples, as seen from comparing the values in

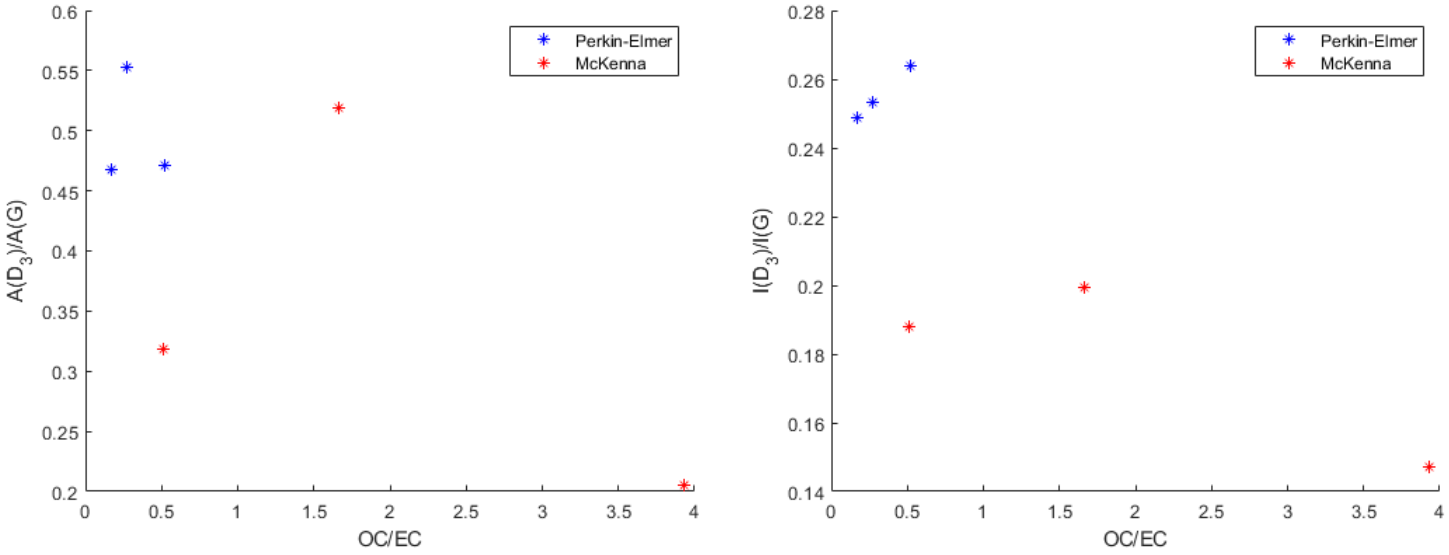

(a) (b)

Figure 29: I_{D_3}/I_G plotted as a function of OC/EC. (a) The area ratio. (b) The height ratio from the fitted data.

Figure 30. This again implies higher maturity for the Perkin-Elmer samples.

Like the MAC, the ratios of the Perkin-Elmer samples have implied that those samples should have lower OC/EC than the McKenna samples. The exception to this is the I_{D_3}/I_G ratios. However, as the exact correlation between I_{D_3}/I_G and OC/EC is not as clear as relation between OC/EC and I_{D_1}/I_G or $\ln(m/I_G)$, so I_{D_1}/I_G and $\ln(m/I_G)$ indicate the correlation more reliably. Therefore, the results from the ratios seem to validate that there is something with the burners that causes the results to not act as predicted when the results are compared between burners.

4 Conclusion and outlook

The peak ratios of this study were obtained either through the heights of the peaks or the areas of the peaks. The results from these ratios imply that salt addition to the fuel used to generate soot decreases the structural order, increases the amount of amorphous carbon, and decreases the bonded hydrogen content of the soot. The first two results indicate that the soot samples with added salt act as less mature soot than the reference soot, and both overall indicates an increase of disorder in the structure of soot. The last result implied that they were more mature than the reference, though it was suggested that the lower hydrogen content can be due to the salt making it harder for hydrogen to bond to the carbon in the sample. Which salt sample had the largest impact on the soot was not consistent for the different methods of obtaining the ratios, aside from the m/I_G ratio, for which the ratio was consistently smaller with the addition of KCl compared to NaCl.

Overall, the addition of the salts did not seem to influence how the soot changes during heating in different atmospheres, or at least no conclusion could be drawn whether the changes observed were significant. In some cases, the heating step in which the ratio started to increase/decrease was different for the samples, but it was not obvious if it was due to a change caused by the salts or the uncertainty in the ratios. For the I_{D_1}/I_G and m/I_G ratios, they usually decreased during the start of the heating, but at higher temperatures they increased. The opposite change was found for the I_{D_3}/I_G ratios. These results imply that order and hydrogen

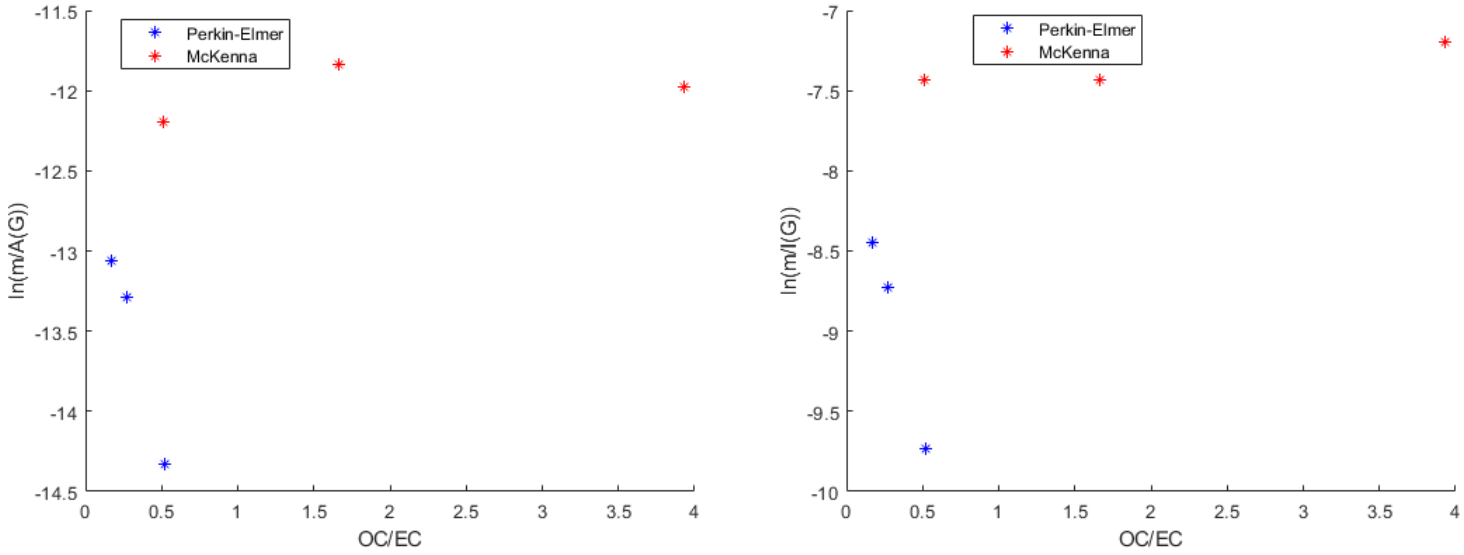

(a)

(b)

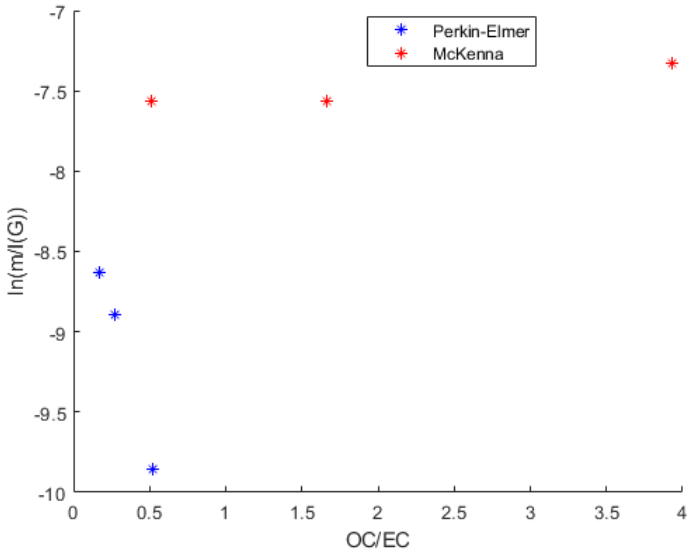

(c)

Figure 30: $\ln(m/I_G)$ plotted as a function of OC/EC. (a) The area ratio. (b) The height ratio from the fitted data. (c) The height ratio from the real height of the peaks.

content decreased at lower heating temperatures and increased at higher temperatures. What part the environments in the heating stage played in the change is not certain.

From the McKenna samples with known relations to their ratios, some of the ratios did not act as predicted, implying that all of the ratios from the Raman measurement were sensitive. However, it was also argued that the differences could be due to outliers in the averaged McKenna samples. One example given was that the averaged 9 mm sample was poor due to the measurements differing significantly. There was also a suggestion that the outliers could be because of the 12 mm sample, where the height of D_1 peak was observed to be significantly smaller than the other peaks, and that its G peaks was significantly thinner. When comparing the ratios of the Perkin-Elmer samples with results from other studies, it was found that the results for these samples were similar, suggesting that the outcomes in this case were not significantly altered by outliers.

The OC/EC ratio acted as predicted for the samples. The OC/EC ratios for the Perkin-Elmer samples were overall lower than the McKenna samples and were higher for the samples with salt addition, with the KCl having a higher ratio. The OC/EC ratio overall is sensitive, but due to the difference between the two samples with salt addition and the reference sample being significant, it was suggested that the samples with salt addition acted as combustion catalysts and limits the soot particle size of the sample, causing the OC/EC ratio results. The MAC was found to decrease with the addition of salt and lower HAB. The KCl sample had a lower MAC than the other Perkin-Elmer samples.

This study contributes to the understanding salt's effects on soot. While it shows some promising results, the sensitivity of the ratios and the inherent inaccuracy that comes with deconvolution means that there could be flaws in the results. Therefore, more studies need to be conducted to verify whether these results are accurate or not. Also, more studies need to be done to see whether the small differences in how the samples with salt addition and the reference sample change during the heating protocol are significant or not. Whether the environment in which the heating occurs also gives different results can also be interesting to follow up on. It might also be of interest to try to calculate a more accurate MAC by measuring the f for the different samples, as it was assumed to be the same for all samples.

During the project, there were a lot of discussions on what else to include for this thesis, but could not be done due to the limited time. One of the more interesting things that were discussed is that maybe the amount of salt added to the soot could influence the soot differently. There was also concern about time and whether more measurements on the same sample could be done. If more measurements of the same samples are gathered for the average Raman spectra, it could mean more accurate results. Gathering more measurements may also allow for the dismissal of poor measurements without affecting the spectra too much. Though there is always going to be an uncertainty due to the deconvolution, errors from that can be resolved by gathering more data.

Acknowledgements

I would like to thank my supervisors, Thi Kim Cuong Le and Saga Bergqvist for help and support during my thesis work. Bergqvist gave me some hints for the data analysis and she along with Jefry John and Le helped me in the lab. Le and Bergqvist also gave feedback on my algorithm for data analysis and guided me when I was not sure what to do. I would like to thank the people at the Combustion physics department, as they made me feel welcomed to their work environment. I would also like to thank Johannes Rex and his team at IKDC, as they performed the thermo-optical-transmission experiment and calculated the OC and EC. Finally, I would like to thank my family and friends, who have supported me as best as they could.

References

[1] S. Szopa et al., "Short-Lived Climate Forcers" in *Climate Change 2021: The Physical Science Basis*, V.Masson-Delmotte et al., Eds. Cambridge, United Kingdom and New York, NY, USA: Cambridge University Press, 2021, ch. 6, pp. 817–922, doi: 10.1017/9781009157896.008.

[2] T. C. Le, J. Henriksson, P-E. Bengtsson, "Polarization effects in Raman spectroscopy of light-absorbing carbon", Jour. Raman Spectrosc., vol. 52, pp. 1115–22, May 2021, doi: 10.1002/jrs.6107

[3] M. Mannazhi, S. Bergqvist, P-E. Bengtsson, "Influence of potassium chloride on PAH concentration during soot formation studied using laser-induced fluorescence", Comb. & Flame, vol. 235, pp. 1-7, Jan. 2022, doi: 10.1016/j.combustflame.2021.111709

[4] H. A. Michelsen et al., "A review of terminology used to describe soot formation and evolution under combustion and pyrolytic conditions", ACS Nano, vol. 14, no. 10, pp. 12470-90, Sep. 2020, doi: 10.1021/acsnano.0c06226

[5] H. A. Michelsen, "Probing soot formation, chemical and physical evolution, and oxidation: A review of in situ diagnostic techniques and needs", Proc. Comb. Inst., vol. 36, no. 1, pp. 717-35, Aug. 2016, doi: 10.1016/j.proci.2016.08.027

[6] K. C. Le et al., "Raman spectroscopy of mini-CAST soot with various fractions of organic compounds: Structural characterization during heating treatment from 25 °C to 1000 °C", Comb. & Flame, vol. 209, pp. 291-302, Nov. 2019, doi: 10.1016/j.combustflame.2019.07.037

[7] E. J. Highwood, R. P. Kinnersley, "When smoke gets in our eyes: The multiple impacts of atmospheric black carbon on climate, air quality and health", Envir. Int., vol. 32, no. 4m pp. 560-6, May 2006, doi: 10.1016/j.envint.2005.12.003

[8] S. Török, "Optical investigations and characterization of soot of different morphology and maturity", Ph.D. dissertation, Dept. Phys., Lund Univ., Lund, Sweden, 2021

[9] K. Gao, F. Friebel, C-W. Zhou, Z. A. Kanji, "Enhanced soot particle ice nucleation ability induced by aggregate compaction and densification", ACP, vol. 22, no. 7, pp. 4985–5016, Apr. 2022, doi: 10.5194/acp-22-4985-2022

[10] T. C. Bond et al., "Bounding the role of black carbon in the climate system: A scientific assessment", JGR Atmos., vol. 118, no. 11, pp. 5380-552, Jan. 2013, doi: 10.1002/jgrd.50171

[11] J. Hansen, L. Nazarenko, "Soot climate forcing via snow and ice albedos", PNAS, vol. 101, no. 2, pp. 423-8, Dec. 2003, doi: 10.1073/pnas.2237157100

[12] J. Simonsson, N. E. Olofsson, A. Hosseinnia, P. E. Bengtsson, "Influence of potassium chloride and other metal salts on soot formation studied using imaging LII and ELS, and TEM techniques", Comb. & Flame, vol. 19, pp. 188-200, Apr. 2018, doi: 10.1016/j.combustflame.2017.11.020

[13] M. Mannazhi et al., "Strongly reduced optical absorption efficiency of soot with addition of potassium chloride in sooting premixed flames", Proc. Comb. Inst., vol. 39, no. 1, pp. 867-76, Sep. 2022, doi: 10.1016/j.proci.2022.07.143

[14] A. Sadezky, H. Muckenhuber, H. Grothe, R. Niessner, U. Pöschl, "Raman microspectroscopy of soot and related carbonaceous materials: Spectral analysis and structural information", Carbon, vol. 43, no. 8, pp. 1731-42, July 2005, doi: 10.1016/j.carbon.2005.02.018

[15] G. De Falco, S. Bocchicchio, M. Commodo, P. Minutolo, A. D'Anna, "Raman spectroscopy of nascent soot oxidation: structural analysis during heating", Front. Energy Res., vol. 10, pp. 1-11, June 2022, doi: 10.3389/fenrg.2022.878171

[16] M. Pawlyta, J-N. Rouzaud, S. Duber, "Raman microspectroscopy characterization of carbon blacks: Spectral analysis and structural information", Carbon. vol. 84, pp. 479-90, April 2015, doi: 10.1016/j.carbon.2014.12.030

[17] S. Chen et al., "Thermal conductivity measurements of suspended graphene with and without wrinkles by micro-Raman mapping", Nanotech., vol. 23, no. 36, pp. 1-4, Aug. 2012, doi: 10.1088/0957-4484/23/36/365701

[18] S. Bocchicchio et al, "Thermo-optical-transmission OC/EC and Raman spectroscopy analyses of flame-generated carbonaceous nanoparticles", Fuel, vol. 310, pp. 1-10, Feb. 2022, doi: 10.1016/j.fuel.2021.122308

[19] J. Henriksson, "Raman spectroscopy for characterization of soot and other carbonaceous materials", M.S thesis, Dept. Phys. Div. Comb. Phys., Lund Univ., Lund, Sweden, 2019

[20] L-W. A. Chen et al., "Multi-wavelength optical measurement to enhance thermal/optical analysis for carbonaceous aerosol", Atmos. Meas. Tech., vol. 8, no. 1, pp. 451–461, Jan. 2015, doi: 10.5194/amt-8-451-2015

[21] J. C. Chow et al., "Optical calibration and equivalence of a multiwavelength thermal/optical carbon analyzer", Aeros. Air Quality Res., vol. 15, no. 4, pp. 1145–59, Aug. 2015, doi: 10.4209/aaqr.2015.02.0106

[22] C. Russo, A. Ciajolo, "Effect of the flame environment on soot nanostructure inferred by Raman spectroscopy at different excitation wavelengths", Comb. & Flame, vol. 162, no. 6, pp. 2431-41, June 2015, doi: 10.1016/j.combustflame.2015.02.011

[23] J. C. Chow et al., "Quality assurance and quality control for thermal/optical analysis of aerosol samples for organic and elemental carbon", Analytical & Bioanalytical Chem., vol. 401, pp. 3141–52, May 2011, doi: 10.1007/s00216-011-5103-3

[24] T. Leffler, "Development and application of optical diagnostics of alkali vapours for solid fuel combustion", Doctoral Thesis (compilation), Dept. Phys. Div. Comb. Phys., Lund Univ., Lund, Sweden, 2016

[25] G. Scarlatella, "Development of a schlieren system for a mobile rocket combustion chamber", M.S thesis, Polytechnic Univ. of Turin, Turin, Italy, 2019

[26] F. Cavalli, M. Viana, K. E. Yttri, J. Genberg, J-P. Putaud, "Toward a standardised thermal-optical protocol for measuring atmospheric organic and elemental carbon: the EUSAAR protocol", Atmos. Meas. Tech., vol. 3, no. 1, pp. 79-89, Jan. 2010, doi: 10.5194/amt-3-79-2010

[27] A. C. Ferrari, J. Robertson, "Interpretation of Raman spectra of disordered and amorphous carbon", Phys. Rev. B, vol. 61, no. 20, pp. 14095-107, May 2000, doi: 10.1103/PhysRevB.61.14095

[28] C. Russo, F. Stanzione, A. Tregrossi, A. Ciajolo, "Infrared spectroscopy of some carbon-based materials relevant in combustion: Qualitative and quantitative analysis of hydrogen", Carbon, vol. 74, pp. 127-38, Aug. 2014, doi: 10.1016/j.carbon.2014.03.014

[29] M. N. Ess et al., "In situ Raman microspectroscopic analysis of soot samples with different organic carbon content: Structural changes during heating", Carbon, vol. 105, pp. 572-85, August 2016, doi: 10.1016/j.carbon.2016.04.056

[30] Z. Zaho et al., "Influence of alkali metal Na on coal-based soot production", Fuel, vol. 323, pp. 1-12, May 2022, doi: 10.1016/j.fuel.2022.124327

[31] C. Casiraghi et al., "Bonding in hydrogenated diamond-like carbon by Raman spectroscopy", Diamond & Related Materials, vol. 14, pp. 1098–102, Dec. 2004, doi: 10.1016/j.diamond.2004.10.030

[32] G. A. Kelesidis, C. A. Bruun, S. E. Pratsinis, "The impact of organic carbon on soot light absorption", Carbon, vol. 172, pp. 742-9, Feb. 2021, doi: 10.1016/j.carbon.2020.10.032

[33] P. Minutolo, M. Commodo, A. D'Anna, "Optical properties of incipient soot", Proceedings of the combustion institute, vol. 39, no. 1, pp. 1129-38, June 2023, doi: 10.1016/j.proci.2022.09.019

[34] E. Weingartner et al., "Absorption of light by soot particles: determination of the absorption coefficient by means of aethalometers", Aerosol Science, vol. 34, no. 10, pp. 1445-63, Oct. 2003, doi: 10.1016/S0021-8502(03)00359-8

[35] Y. Liu, C. Song, G. Lv, X. Wang, N. Li, "Virgin and extracted soots in premixed methane flames: a comparison of surface functional groups, graphitization degree, and oxidation reactivity", Energy fuels, vol. 31, no. 6, pp. 6413-21, May 2017, doi: 10.1021/acs.energyfuels.6b03011

[36] A. Nose, M. Hojo, T. Ueda, "Effects of Salts, Acids, and Phenols on the Hydrogen-Bonding Structure of Water-Ethanol Mixtures", J. Phys. Chem. B, vol. 108, no. 2, pp. 798-804, Dec. 2003, doi: 10.1021/jp0308312

[37] H. Bladt, N. P. Ivleva, R. Niessner, "Internally mixed multicomponent soot: impact of different salts on soot structure and thermo-chemical properties", Jour. of aerosol science, vol. 70, pp. 26-35, April 2014, doi: 10.1016/j.jaerosci.2013.11.007.

[38] T. Haller et al., "Structural changes of CAST soot during a thermal–optical measurement protocol", Atmos. Meas. Tech., vol 12, no. 7, pp. 3503–19, Jul 2019, doi: 10.5194/amt-12-3503-2019